

Electronic structure and density of states of the random $\text{Al}_{0.5}\text{Ga}_{0.5}\text{As}$, $\text{GaAs}_{0.5}\text{P}_{0.5}$, and $\text{Ga}_{0.5}\text{In}_{0.5}\text{As}$ semiconductor alloys

Rita Magri, Sverre Froyen, and Alex Zunger

Solar Energy Research Institute, Golden, Colorado 80401

(Received 8 February 1991)

The electronic density of states (DOS), charge densities, equilibrium bond lengths, and optical bowing of the direct band gaps are calculated for three perfectly random semiconductor alloys within the first-principles pseudopotential method using the concept of "special quasirandom structures" (SQS's). The SQS's are periodic structures with moderately large unit cells whose sites are occupied by atoms in a way designed to reproduce the structural features of the infinite, perfectly random substitutional alloys. In avoiding averaging over atoms (as in the virtual-crystal approximation) or over atomic environments (as in the site-coherent-potential approximation), this approach is capable of revealing the multisite nature of chemical disorder, as well as atomic-relaxation effects. We show how the existence of different local environments about chemically identical sites leads to splittings and fine structures in the density of states, and how atomic relaxations are induced by such nonsymmetric environments and lead to significant modifications in these DOS features. The calculated alloy bond lengths and optical-bowing coefficients are found to be in good agreement with experiment. Relaxation-induced splittings in the DOS are offered as predictions for future photoemission studies.

I. INTRODUCTION

Isovalent zinc-blende AC and BC semiconductors tend to form stable and continuous substitutional solid solutions $A_{1-x}B_xC$ when grown above the miscibility gap temperature.¹⁻³ X-ray diffraction,¹⁻⁴ nuclear-magnetic-resonance chemical-shift measurements,⁵ Raman scattering,⁶ and extended x-ray-absorption fine-structure (EXAFS) experiments⁷⁻⁹ show that while low-temperature vapor-phase growth often leads to substantial deviations from randomness (e.g., to short-range clustering^{4,6} or even to long-range ordering¹⁰), liquid-phase or melt-grown alloys tend to organize microscopically in near-random atomic arrangements.¹⁻⁴ There, the occupations of the "mixed sublattice" (A and B) follow closely Bernoulli's random (R) statistics. For example, the different C -centered nearest-neighbor atomic tetrahedra A_4 , A_3B , A_2B_2 , AB_3 , and B_4 appear at alloy concentration x in the relative ratios given by^{5,8} $P_R^{(n)}(x) = \binom{4}{n} x^n (1-x)^{4-n}$, where n is the number of A atoms in the $A_n B_{4-n}$ cluster. Similarly,⁵ the twelve $A_m B_{12-m}$ arrangements of the next-nearest neighbors about A occur in the relative proportions $P_R^{(m)} = \binom{12}{m} x^m (1-x)^{12-m}$. Indeed, the existence of such *distributions* of "local environments" about sites is the hallmark of disordered alloys, distinguishing them from ordered intersemiconductor compounds (e.g., short-period superlattices, where only a small number of cluster types exist), or from the pure binary AC and BC constituents (where only A_4 or B_4 clusters occur). These non-periodic *distributions* of local environments lead to changes in the physical properties (alloy band gaps, effective masses, density of states, bond lengths) and consequently to the technologically attractive possibility of tuning these properties with x to meet desired

specifications.

Understanding the fashion in which such nonperiodic cluster distributions control optical and structural alloy properties has been the focus of much of the theoretical research both of metal^{11,12} and of semiconductor¹³ alloys. As translational invariance is lost, Bloch-periodic functions such as band structures are replaced by statistical constructs including density of states (DOS), local DOS (LDOS), spectral functions, and average bond lengths. We know that at a composition x there are $N!/(xN)!(1-x)N!$ ways of distributing the A and B atoms on the N available lattice sites; each such configuration is distinguished from others by having different local environments. Even though the *occupations* of the different sites in a configuration may be (e.g., by construction) perfectly random, the *properties* of the already occupied sites need not follow random statistics. For example, a C atom coordinated locally by four A atoms could have a different charge transfer or local bond lengths than a C atom coordinated locally by, say four B atoms.¹⁴ The fact that such chemically identical atoms may, in general, have different local environments (i.e., be structurally inequivalent), does not of course affect the properties that depend only on the *global* alloy composition (e.g., the molecular weight of $A_{1-x}B_xC$). Yet, physical properties that involve *local* coupling between atoms (e.g., charge transfer, bond relaxation) may exhibit finite (nonrandom) correlations even in nominally (occupation-wise) random alloys. For example, the configurational average of the product of charges on two sites $\langle Q_i Q_j \rangle$ (which determines electrostatic energies) is *not*¹⁴ $\langle Q_i \rangle \langle Q_j \rangle = 0$, even though the *occupation* variables of a perfectly random alloy are uncorrelated, i.e., $\langle S_i S_j \rangle = \langle S_j \rangle \langle S_i \rangle$. Since macroscopic observables correspond to averages over all configurations, the central question here is the extent to which environmental fluct-

tuations in different properties survive averaging. The various theoretical approaches applied previously to describe the electronic structure of random alloys differ in their treatment of this issue.

The virtual-crystal approximation¹⁵ (VCA) averages the potentials of all atoms in the alloy, hence, *all* fluctuations are lost. The failure of the VCA in accounting for distinct *A*-like or *B*-like spectral features is well documented for both semiconductor^{13,16} and metal¹¹ alloys. The site-coherent-potential approximation¹⁷ (SCPA) retains the separate identities of the *A* and *B* sublattices but average over the environments of each site. Since it assumes that random *occupations* of sites also implies that the physical properties of the sites are uncorrelated (e.g., that $\langle Q_i Q_j \rangle = \langle Q_i \rangle \langle Q_j \rangle = 0$), all *C* atoms (and separately, all *A* or *B* atoms) are assumed to scatter electrons equivalently. While this approximation captures some “chemical disorder” effects due to the different potentials on *A* and *B* (see applications of the CPA in Refs. 18–20 to $A_{1-x}B_xC$ semiconductor alloys), it misses distinct environmental effects^{19,21} associated with the existence of a different distribution of *A* (and separately *B*) atoms. The molecular CPA (Refs. 19 and 22) (MCPA) retains a longer correlation length over which structural and chemical characteristics are retained. This often leads to additional structure¹⁹ in the DOS. The supercell approach^{23–27} considers a crystallographic unit cell whose sites are occupied by atoms in a manner aimed at reproducing approximately a random alloy. The electronic structure is then solved (either with periodic^{26,27} or with free-cluster^{24,25} boundary conditions) using any of the available electronic-structure methods. Correlation between the properties of different sites are permitted (and are limited in extent by the supercell size). A distribution of various local environments is naturally included. This resolves even more DOS features than the MCPA; examples include large ($N \sim 10^3$ atoms/cell) randomly occupied supercells treated by tight-binding recursion methods^{24,25} and the 16-atom chalcopyrite model of zinc-blende alloys treated by first-principles density-functional methods.²⁷ Even more detailed representations of alloy environmental effects were obtained by performing a set of different supercell calculations, each representing a distinct (repeated) cluster, and superposing those according to the statistical probabilities in which the underlying clusters appear in an infinite random alloy. Such approaches have been applied to study spin-orbit splitting²⁸ and band-gap bowing²⁹ in II-VI and III-V alloys.

The computational complexity of the SCPA,^{18–20} MCPA,^{19,22} and large-supercell approaches^{23–25} has limited their application for semiconductor alloys to simplified electronic models, mostly empirical tight-binding methods. On the other hand, while small supercell approaches were applied in the context of more sophisticated first-principles electronic structure methods,^{26,27,28(b),29(b),29(c)} the small number of atoms used to model a random alloy (and their high-symmetry arrangements) could misrepresent the correct statistical structure.

We have recently developed^{30,31} a systematic method

of constructing small supercells whose sites are occupied by atoms in a manner designed to reproduce approximately the structure of an infinite random alloy. The atomic structure of an infinite, perfectly random alloy with a given Bravais lattice (e.g., fcc) and composition x is characterized by its many-body correlation functions³¹ $\langle \bar{\Pi}_{k,m}(x) \rangle$. We consider “clusters” consisting of k atoms separated by up to m th-neighbor distances. We then search for a single ordered, N -atom supercell whose correlation functions $\bar{\Pi}_{k,m}(N)$ have minimal deviations from $\langle \bar{\Pi}_{k,m}(x) \rangle$ up to a given order in (k, m) . Interestingly, such “special quasirandom structures” (SQS’s) with only eight *A* and *B* atoms per cell already reproduce rather accurately^{30,31} the first few (physically most significant) random correlation functions $\langle \bar{\Pi}_{k,m} \rangle = (2x - 1)^k$. Here, the constraint of matching the first few correlation functions of the infinite, perfectly random alloy *requires* that some chemically identical sites be crystallographically inequivalent; any other occupation scheme in a small supercell results, by necessity, in a worse description of the real random alloy. In this paper we use a self-consistent pseudopotential description of the properties of $\text{Al}_{0.5}\text{Ga}_{0.5}\text{As}$, $\text{In}_{0.5}\text{Ga}_{0.5}\text{As}$, and $\text{GaP}_{0.5}\text{As}_{0.5}$ random alloys modeled by the SQS8. The general properties of such SQS’s (Refs. 30 and 31) and their applications to II-VI semiconductor alloys³² and some transition-metal alloys³³ were described previously.

II. METHOD OF CALCULATION

The SQS8 is a $(AC)_1/(BC)_2/(AC)_3/(BC)_2$ superlattice in the [113] direction with four *A*, four *B*, and eight *C* atoms per unit cell. Detailed information about the lattice vectors and the atomic positions inside the unit cell for this structure were given elsewhere.^{30,31} The SQS8 has two variants, obtained by switching the *A* and *B* atoms (denoted as SQS8_a and SQS8_b). For completely relaxed structures we find that the formation enthalpies of these variants differ by as little as 1 meV/atom pair while the minimum direct band gaps at Γ differ by only 0.01 eV. As noted above, the atomic sites within the SQS unit cell are structurally inequivalent. Considering first the nearest neighbors to the common atom *C*, we see different coordinating atoms: in SQS8_a we have the *C*-centered clusters A_4 , A_3B , A_2B_2 , and AB_3 with the relative frequency 1:1:3:3 in the complementary SQS8_b we have the clusters B_4 , AB_3 , A_2B_2 , and A_3B (with the same frequencies). Notice therefore that the occurrence of the $A_n B_{4-n}$ clusters with $n = 4, 3, 2, 1$, and 0 around the *C* atoms follows the random probability at composition $x = \frac{1}{2}$ (ratios of 1:4:6:4:1) if we consider SQS8_a and SQS8_b together. Considering next second neighbors, the *A* and the *B* atoms again have different environments. For example, in SQS8_a there are two inequivalent *B* atoms: $B^{(5)}$, surrounded in the second shell by five *A* and seven *B* atoms and $B^{(7)}$, surrounded by seven *A* and four *B* atoms. Again the *average* number of atoms of opposite type to that at the origin follows closely the average value in the random alloy.^{30,31}

We studied the electronic structure of the SQS using the first-principles, self-consistent pseudopotential ap-

proach³⁴ with nonlocal pseudopotentials constructed by the approach of Kerker.³⁵ Exchange and correlation effects were treated within the local-density approximations using the Ceperley and Alder³⁶ potential as parametrized by Perdew and Zunger.³⁷ The wave functions were expanded in a basis set with about 150 plane waves per atom (kinetic energy cutoff of 15 Ry). Brillouin-zone integrations were performed by Fourier quadrature using a set of 21 k points equivalent to 29 fcc special points.³⁸ For the DOS calculation the eigenvalues are obtained directly at a set of 73 k points (equivalent to 85 zinc-blende k points), including high-symmetry points. We have checked the convergence of the results as a function of the number of k points and find that a larger set consisting of 146 k points gives the same DOS peak positions to within 0.05 eV. The eigenvalues were then linearly interpolated on a denser k -point mesh using the tetrahedron interpolation scheme.³⁹ For the local DOS calculations each energy was weighted with a weight equal to the projection of the corresponding wave function in a Wigner-Seitz sphere around an atom. The Wigner-Seitz radii depend on the equilibrium volume and are 3.23, 3.29, and 3.41 a.u. for GaAs_{0.5}P_{0.5}, Al_{0.5}Ga_{0.5}As, and Ga_{0.5}In_{0.5}As, respectively. Since LDOS results depend on these radii, they are quoted in what follows only in “arbitrary units.”

The equilibrium atomic positions for the lattice-mismatched systems Ga_{0.5}In_{0.5}As and GaAs_{0.5}P_{0.5} were determined by minimizing the total energy with respect to the cell-internal structural parameters, retaining the cubic unit cell dimensions. The calculated equilibrium lattice constants were within 0.2% of the average of the calculated values for the two zinc-blende constituents (Vegard’s rule). A fully relaxed configuration was obtained through an iterative process using first-principles calculated forces and an approximate force constant matrix based on Keating’s⁴⁰ valence force-field model. The final (zero-force) geometry does not depend on the force constants used; only the convergence rate of the iterative

relaxation is. Because of the structural inequivalence of atoms of the same chemical identity, the relaxed SQS8 manifests a *distribution* of bond lengths for each (e.g., $A-C$ or $B-C$) atom pair. Table I compares the calculated average nearest-neighbor bond lengths \bar{d} in SQS8 with the virtual-lattice average $d_{\text{VLA}} = xd_{A-C}^0 + (1-x)d_{B-C}^0$ and with the values d^0 in the binary constituents. The alloy values \bar{d} deviate substantially from the virtual-lattice average values and are closer to the binary equilibrium bond lengths. As seen in Table I, the magnitudes of these deviations agree well with those found in EXAFS measurements on these systems.^{7,9}

III. GENERIC FEATURES IN THE DOS OF III-V ZINC-BLENDE COMPOUNDS

We start our discussion of the DOS by establishing the basic features of the DOS of a pure III-V zinc-blende compound; this will serve below as a benchmark for assessing alloy effects on the states of a pure compound. An analogous discussion for II-VI compounds was given in Ref. 32.

We use AlAs as an example for III-V compounds. Figure 1 gives the calculated total DOS of AlAs. It exhibits three distinct valence-band peaks denoted $P1$, $P3$, and $P4$ and two conduction-band peaks denoted $P5$ and $P6$. For notational compatibility with Ref. 32 we have omitted $P2$: this state corresponds to the metal d states; in II-VI semiconductors³² they are positioned energetically between $P1$ and $P3$, whereas in III-V semiconductors they lie deeper than⁴¹ $P1$ and hence will not be considered here.

Figure 2 depicts the electronic charge densities in energy regions corresponding to these peaks, while Fig. 3 gives the site and angular momentum decomposed LDOS. From these data we can characterize the localization and hybridization of each generic DOS peak as follows.

- (i) $P1$ is an isolated band around $E_v - 11$ eV consisting of

TABLE I. Calculated bond lengths for the binary zinc-blende constituents (d_{binary}^0), the $x = \frac{1}{2}$ virtual-lattice average (VLA) $d_{\text{VLA}} = \frac{1}{2}d_{A-C}^0 + \frac{1}{2}d_{B-C}^0$, and the average (with fluctuation denoted as \pm) over the distribution of bond lengths in SQS8_a and SQS8_b (\bar{d}_{SQS8}). The quantity $d^0 - \bar{d}$ gives the predicted change in bond length in the $x = \frac{1}{2}$ alloy relative to the pure constituents. Since the local density method used here makes a small error in d_{binary}^0 , we calculate the predicted alloy bond length by subtracting our LDA-calculated $d^0 - \bar{d}$ value from the *measured* d_{binary}^0 (2.448, 2.623, and 2.360 Å in GaAs, InAs, and GaP, respectively). This gives our predicted alloy bond lengths d_{pred} that are compared to the EXAFS-measured values given in the last column.

Bond	d_{binary}^0 (Å)	d_{VLA} (Å)	\bar{d}_{SQS8} (Å)	$d^0 - \bar{d}$	d_{pred}	Expt.
Ga _{0.5} In _{0.5} As						
Ga—As	2.433	2.525	2.449±0.015	−0.016	2.464	2.46 ^a
In—As	2.616	2.525	2.595±0.011	0.021	2.602	2.608 ^b
GaAs _{0.5} P _{0.5}						
Ga—As	2.433	2.387	2.419±0.006	0.014	2.434	2.43 ^c
Ga—P	2.341	2.387	2.354±0.006	−0.013	2.373	2.38 ^c

^aReference 9(b).

^bReference 7.

^cReference 9(a).

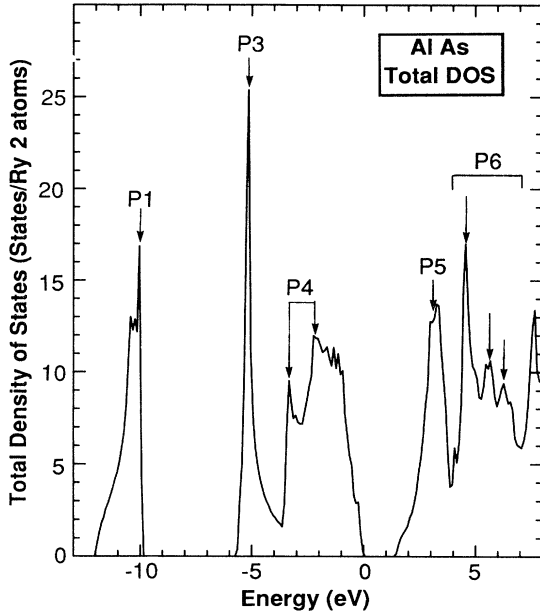


FIG. 1. Total density of states of AlAs at the cubic lattice constant $a = 5.619 \text{ \AA}$, labeling the various “generic” peaks discussed in the text (Sec. III).

an atom-centered anion s valence state. It contains a small admixture of states with s , p , and d character about the cation sites.

(ii) $P3$ is an sp^3 -like bonding valence state evolving largely from cation s and anion p orbitals. It is spatially localized on the anion-cation bond with a peak charge density polarized towards the anion site.

(iii) $P4$ is a spatially extended anion p , d and cation p , d bonding valence state. Its peak charge density is near the anion site along the anion-cation $[111]$ bond direction.

(iv) $P5$ is the antibonding of sp^3 -like counterpart of the $P3$ state. It is composed from cation s , p , d and anion s ,

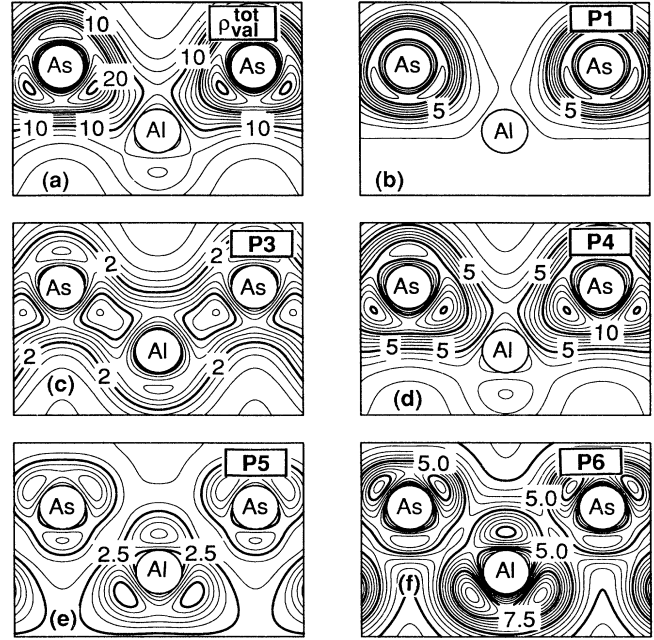


FIG. 2. Contour plots of the electronic charge densities in the (110) plane for the main peaks in the DOS of AlAs (Fig. 1). (a) Total valence pseudo-charge-density, (b) $P1$, (c) $P3$, (d) $P4$, (e) $P5$, and (f) $P6$. The peaks $P1$ – $P4$ represent valence bands whereas $P5$ and $P6$ are conduction bands. The contour steps in (a)–(f) are, respectively, 2, 1, 0.4, 1, 0.5, and 0.5 (in units of electrons per unit cell volume).

p , d orbitals and is spatially localized on the “antibond” $[\bar{1}\bar{1}\bar{1}]$ direction with a node along the bond.⁴²

(v) $P6$ is a spatially extended antibonding conduction state made of cation p , d and anion p , d orbitals. Like $P5$ but unlike $P3$, its charge density lobes point away from the nearest-neighbor bonds.

The DOS features discussed above for AlAs appear similarly in all other III-V semiconductors. Table II

TABLE II. Peak positions (indicated by arrows in Fig. 1) in the density of states of the binary compounds GaAs, AlAs, InAs, GaP, for different values of the lattice parameters. We use the calculated lattice constants for the binary constituents and for the corresponding alloys. Energies are given in eV relative to the valence-band maximum.

System	Peak energies (eV)							
	$P1$	$P3$	$P4$	$P5$	$P6$			
GaAs, $a = a_{\text{GaAs}}$	-10.4	-6.5	-3.7	-2.6	2.5	4.5	5.6	7.6
GaAs, $a = a_{\text{GaInAs}}$	-10.2	-6.1	-3.3	-2.3	2.3	4.4	5.4	7.2
GaAs, $a = a_{\text{GaAsP}}$	-10.6	-6.8	-4.0	-2.8	2.6	4.5	5.6	7.8
AlAs, $a = a_{\text{AlAs}} \approx a_{\text{GaAs}}$	-10.0	-5.1	-3.3	-2.2	3.3	4.5	5.6	7.6
InAs, $a = a_{\text{InAs}}$	-10.1	-5.6	-3.1	-2.2	2.4	4.3	5.3	6.9
InAs, $a = a_{\text{GaInAs}}$	-10.5	-6.1	-3.7	-2.6	2.6	4.4	5.5	7.4
GaP, $a = a_{\text{GaP}}$	-9.6	-6.4	-3.8	-2.6	2.9	4.5	5.7	7.8
GaP, $a = a_{\text{GaAsP}}$	-9.4	-6.2	-3.5	-2.5	2.7	4.5	5.5	7.6

gives the peak positions in GaAs, GaP, and InAs for a number of unit cell volumes pertinent to the alloys discussed here. Note the systematic trends in Table II, e.g., the phosphoruslike $P1$ peak in GaP has lower binding energy than the arseniclike $P1$ peak in GaAs, and the Ga-like $P3$ peak is deeper in GaAs than the corresponding Al-like $P3$ peak in AlAs. When these band energies are aligned on an absolute energy scale (using band offsets), the trends correlate with the pertinent atomic orbitals energies (see the Appendix^{43–35}).

IV. METHOD OF ANALYSIS OF ALLOY-INDUCED DOS CHANGES

Having established the nature of the DOS features in pure III-V compounds treated here, we describe next the methodology we use to analyze alloying effects on these states. Since we wish to discern the effect of structural perturbations from those of chemical perturbations, we use the following sequence of calculations.³²

(i) *Volume-deformation effects:* Since the molar volume of a $A_{1-x}B_xC$ alloy is intermediate between those of the AC and BC constituents (usually² close to the concentration-weighted average denoted \bar{V}), in size-mismatched alloys the volume of the smaller component

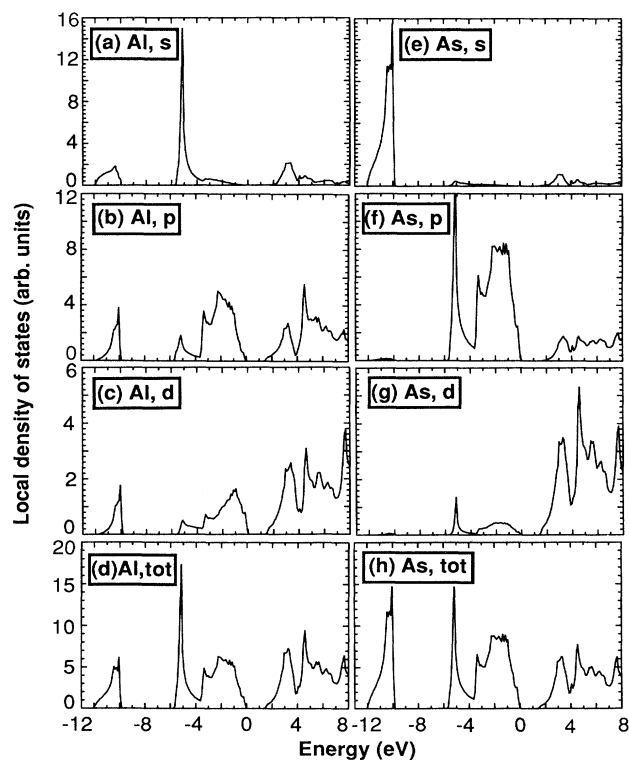


FIG. 3. Atom and angular momentum resolved local density of states in cubic AlAs. This information is used in Sec. III along with the charge density plots of Fig. 2 to characterize the orbital nature of each generic DOS structure.

expands while that of the larger component contracts. Finite hydrostatic deformation potentials⁴⁶ then couple such volume changes to the electronic states, as shown in Fig. 4. We see that the *bonding* states $P1$, $P3$, and $P4$ are displaced upon volume expansion into *smaller* binding energies [Figs. 4(a) and 4(d)], whereas volume contraction moves bonding states into *larger* binding energies [Figs. 4(b) and 4(c)]. Conversely, the *antibonding* $P5$ and $P6$ states drop in energy upon volume expansion [Figs. 4(a) and 4(d)], while volume contraction increases their energies [Figs. 4(b) and 4(c)]. These effects are well understood in terms of the response of tight-binding states⁴¹ to hydrostatic deformations.⁴⁶ Table II gives these calculated shifts for the alloys studied here.

(ii) *Virtual-crystal effects:* In the next step of the calculation we construct a virtual lattice from the constituents AC and BC that are already prepared at the alloy's calculated molar volume \bar{V} (or lattice constant \bar{a}). A direct pseudopotential calculation of the bands of a virtual zinc-blende structure with concentration-weighted potentials of the deformed constituents gives the DOS in this “virtual-crystal approximation.” All bond lengths are equal to $\sqrt{3}\bar{a}/4$ and all bond angles are kept at their tetrahedral values. Since in this approximation the zinc-blende symmetry is imposed, the DOS has precisely the same topological features as in the pure zinc-blende components. The AC - BC band splittings deducible by comparing the corresponding DOS structures of AC and BC compounds in Fig. 4 are hence eliminated. In this approximation, both “structural disorder” (resulting from

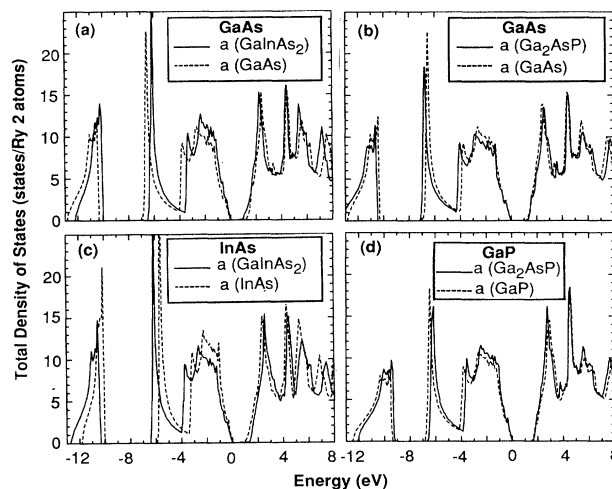


FIG. 4. Volume-induced hydrostatic shifts in the total density of states of zinc-blende semiconductors. The dashed lines give the DOS at the calculated equilibrium lattice constant of the binary semiconductors, whereas the solid lines give the DOS of the same semiconductor but at the corresponding alloy volume. The calculated equilibrium bond lengths are given in Table I. Note that upon lattice dilation, bonding states such as $P3$ are displaced to deeper binding energies, whereas antibonding states such as $P5$ are displaced to lower binding energies. The zero of energy is taken at the valence-band maximum.

dissimilar bond lengths and angles) and “chemical disorder” are excluded by construction. Note that we include the VCA step only as a benchmark against which other results can be compared, not as a viable alloy theory.

(iii) *Chemical-disorder effects:* We next calculate the DOS in the SQS8 model at the volume \bar{V} , keeping however all bond lengths and angles equal to those in the virtual lattice (“unrelaxed SQS”). Like in the VCA calculations of step (ii), structural disorder is excluded, but unlike it, chemical disorder effects are included: distinct A and B atoms are retained with no averaging. Note that unlike the SCPA, this model retains the chemical fluctuations arising from the existence of different A and, separately, different B sites. A recent test²⁵ compared the results of this model in the context of a tight-binding description to those obtained in the SCPA (where all A atoms are averaged and so are all B atoms) for a case where structural disorder is negligible (the lattice-matched $\text{Al}_{0.5}\text{Ga}_{0.5}\text{As}$ system). It was found that the SCPA captures well chemical disorder effects in the spectral ranges where the alloy perturbation is reasonably small (in the Γ_{1c} and X_{1c} regions) but that noticeable differences exist when the perturbation is larger (e.g., in the X_{3c} spectral region). In the later cases, a multisite description of chemical disorder effects (underlying the SQS) is important.

(iv) *Structural-disorder effects:* In the last step we contrast the DOS of the unrelaxed SQS model of step (iii) with that obtained from the SQS whose atomic positions are relaxed to obtain a minimum in the total energy of the cubically shaped cell. The nearest-neighbor A - C and B - C bond lengths (Table I) are no longer equal, as in steps (i)–(iii). Relative to the virtual lattice average, the shorter of the two (AC and BC) bonds become (slightly) shorter, whereas the longer of the two becomes longer (Table I). Such relaxations couple to the electronic states through phononlike deformation potentials,⁴⁷ causing additional shifts and splittings.

Following the analysis above, we will calculate the total DOS of (i) the binary constituents at their equilibrium volumes as well as at the alloy volume, (ii) the VCA density of states, (iii) the unrelaxed SQS density of states and, for lattice-mismatched alloys, (iv) the fully relaxed SQS density of states. This will provide a description of volume deformation as well as chemical and positional disorder effects on the global density of states.

In addition to the *total* DOS, we are interested to explore how “environmental effects” lead to distinct features in the electronic structure. To this end we will project the DOS onto distinct clusters that exist in the SQS. Each “common atom” C in $A_{1-x}B_xC$ is surrounded, in successive shells by the coordination spheres ($A_{4-n}B_n$), (C_{12}), ($A_{12-m}B_m$), for the first, second, and third neighbors, respectively. To delineate the effects of the first coordination sphere, we calculate the five C -centered cluster LDOS corresponding to the clusters $A_{4-n}B_n$ ($0 \leq n \leq 4$), where the contribution of further shells (e.g., $A_{12-m}B_m$) is averaged out. This is obtained by averaging the LDOS on the structurally inequivalent C atoms in SQS8_a and SQS8_b corresponding to the same cluster n . Obviously, the higher the number of configurations of further shells corresponding to a given

cluster n on which it is possible to average, the more accurate is the “average LDOS” obtained. In SQS8 the number of such configurations is limited by the small size of the unit cell. This procedure gives the C -centered nearest-neighbor LDOS denoted $D_C(A_{4-n}B_n)$. A weighted sum $\sum_n w_n D_C(A_{4-n}B_n)$ over these five LDOS’s gives the “average C -atom LDOS,” similar to what can be expected from the SCPA. Similarly, further shell effects are calculated by keeping a fixed $A_{4-n}B_n$ cluster and examining $D_C^{(n)}(A_{12-m}B_m)$ due to variations in the occupations of the third and further cation shells. To examine second-neighbor effects we consider the first coordination shells about A : (C_4), ($A_{12-m}B_m$), (C_{12}), ($A_{6-m}B_m$), . . . and calculate $D_A(A_{12-m}B_m)$ where further shells are again averaged out. Averaging $D_A(A_{12-m}B_m)$ over the possible configurations $\{m\}$ in the second shell gives the “effective” A -atom LDOS. We will see that in some cases a splitting in the *total* DOS is traceable to distinct features in the *cluster* LDOS. This then permits the interpretation of alloy DOS features in terms of such “environmental effects.”

V. RESULTS FOR $\text{Al}_{0.5}\text{Ga}_{0.5}\text{As}$

We first apply our method to the lattice-matched AlAs - GaAs system which manifests only chemical disorder. Figure 5 depicts the DOS of (a) the zinc-blende constituents, (b) the virtual crystal and (c) the SQS structure.

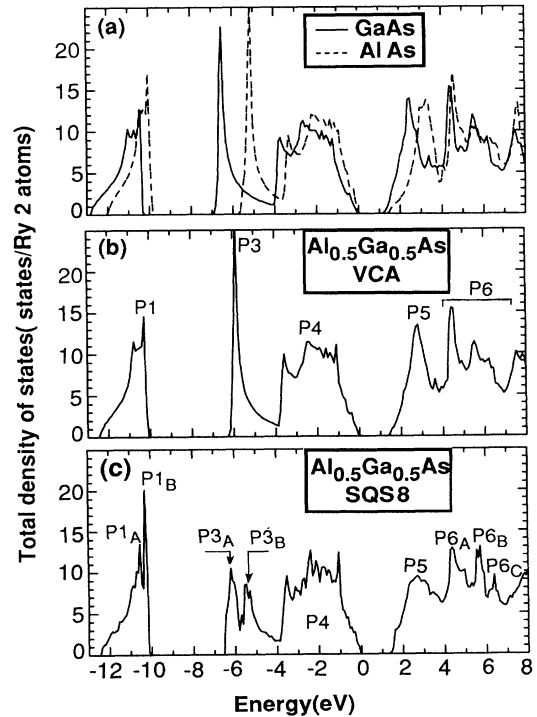


FIG. 5. Total DOS of the AlAs - GaAs system. (a) Binary components, (b) VCA, and (c) average of SQS8_a and SQS8_b .

A. General features

Figure 5(a) and Table II show that when the density of states of GaAs and AlAs are aligned using a common zero of energy (the valence-band maxima), the As-like $P1$ structures and the cationlike $P3$ structures occur at distinctly different energies in the two constituents. Indeed, the substantial difference in the atomic s orbital energies of ^{42}Al and Ga result in a difference of about 1.4 eV in the $P3$ energies in GaAs and AlAs [Fig. 5(a)]. In the VCA [Fig. 5(b)] each As atom is surrounded by four identical “effective” cations, so this approximation is obviously incapable of revealing any “split band” behavior and depicts a single peak for each of the characteristic zincblende DOS structures. In contrast, in the SQS model each As atom has around it some Al and some Ga atoms, so a fraction of the splitting seen in the pure constituents [Fig. 5(a)] is retained in the alloy. Figure 5(c) indeed shows fine structure and splittings, most pronounced in the $P1$, $P3$, and $P6$ regions. The nature of these split bands can be judged by inspection of the electronic

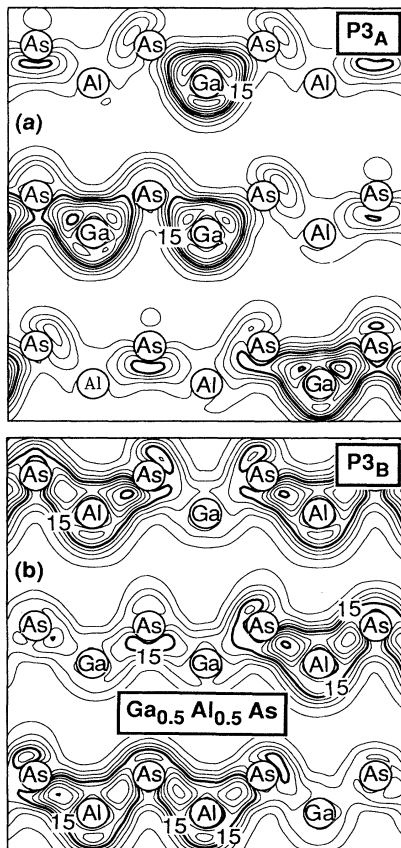


FIG. 6. Electronic charge density contours in the (110) plane for $\text{Al}_{0.5}\text{Ga}_{0.5}\text{As}$ SQS8 in the $P3$ region. (a) $P3_A$ at $E_0 - 6.5$ eV to $E_0 - 5.8$ eV; (b) $P3_B$ at $E_0 - 5.8$ eV to $E_0 - 4.1$ eV. These split peaks in the DOS are seen in Fig. 5(c). Note that $P3_A$ is predominantly an As-Ga state, while $P3_B$ is predominantly an As-Al state. The contour step is 3 (in units of electrons per unit cell volume).

charge density calculated from the wave functions of each split component. Figure 6 shows the charge densities of the $P3_A$ and $P3_B$ peaks, revealing that the deeper $P3_A$ state represents primarily (but not entirely) Ga—As bonds, whereas the lower binding energy $P3_B$ peak represents mostly Al—As bonds. Since each of these subpeaks contains also “minority character” (e.g., Al character in $P3_A$), the splitting in the alloy (0.7 eV) is smaller than that in the pure constituents (~ 1 eV, see the Appendix).

While the Al and Ga atoms differ substantially in their s energies, they have almost identical p energies.⁴³ Thus, the $P4$ and $P5$ DOS structures do not exhibit a strong split-band behavior. In particular, $P4$ displays only fine structure, while $P5$ shows only a broadening. In the two binary compounds the $P5$ peaks are broader and closer to each other (about 0.8 eV) than the corresponding $P3$ peaks. This gives rise in the SQS8 structure to only one very broad structure since, in this case, the two components are not completely resolved. The $P6$ structure, showing two main features in the virtual crystal, exhibits a further splitting of the lower binding-energy component, giving rise to two distinct $P6_B$ and $P6_C$ peaks, more like in the binary AlAs. Analysis of the charge densities analogous to that shown in Fig. 6 reveals that the fine structure of the $P1$ As, s peak is related to the contribution from the different $\text{Al}_n\text{Ga}_{4-n}$, $0 \leq n \leq 4$ local environments about As, affecting the energies of the As, s levels. It is hence natural to analyze the DOS in terms of such clusters.

B. Analysis in terms of the first coordination shell about As

To isolate the effects of the nearest coordination of the As-centered LDOS, we have calculated the DOS of all As-centered clusters and averaged over the next-nearest-neighbor variants present in the SQS8 structure, producing the five density-of-states curves $D_{\text{As}}(\text{Al}_{4-n}\text{Ga}_n)$ associated with the five $\text{Al}_{4-n}\text{Ga}_n$, $0 \leq n \leq 4$ clusters. These are depicted in Figs. 7(a)–7(e). Focusing on the $P3$ region, where the largest variations are apparent, we see a large $P3_B$ intensity in the LDOS corresponding to the Al_4 cluster [Fig. 7(a)]. The intensity of this $P3_B$ component diminishes as the number of Al atoms in each cluster decreases in the series $\text{Al}_4 \rightarrow \text{Al}_3\text{Ga}_1 \rightarrow \text{Al}_2\text{Ga}_2 \rightarrow \text{Al}_1\text{Ga}_3 \rightarrow \text{Ga}_4$ [Figs. 7(a)–7(e), respectively]. Similarly, the intensity of the larger binding-energy component $P3_A$ is small in the Al_4 cluster; it increases as the Ga content of the cluster increases until in the Ga_4 cluster [Fig. 7(e)] this peak is dominant. Clearly, the intensities of the various substructures in the $P3$ region reflect local environmental effects about the As site even though the alloy considered here has a fixed global composition $x = \frac{1}{2}$. Superposition of all five LDOS of Figs. 7(a)–7(e) with the random probability ratios 1:4:6:4:1 for $n = 0, 1, 2, 3, 4$, respectively, produces [Fig. 7(f)] the average contribution of the anion to the DOS.

C. Analysis of further-neighbor effects

As indicated above, each of the five first-neighbor clusters $\text{Al}_{4-n}\text{Ga}_n$ appears in the SQS in a number of variants distinguished by the occupations of the next-neighbor sites. While we have averaged these out in Fig. 7, we now focus on such further-neighbor effects on the DOS. Third and further odd-shell neighbor effects about the As at the origin are apparent when one fixes a given first-neighbor cluster ($\text{Al}_{4-n}\text{Ga}_n$ at a given n) and examines the differences in the LDOS's due to various occupations in the further shells. Figure 8 shows $D_{\text{As}}^{(1)}(\text{Al}_{12-m}\text{Ga}_m)$ for fixed ($n=1$) Al_3Ga_1 nearest-neighbor cluster and varying the third-shell occupations $m=5$ [Figs. 8(a) and (b)], $m=6$ [Fig. 8(c)] and $m=7$ [Fig. 8(d)]. The common characteristic of the $D_{\text{As}}^{(1)}(\text{Al}_{12-m}\text{Ga}_m)$ density of states is that the $P3_A$ peak (Ga-like) is weaker than the $P3_B$ peak (Al-like). The shape and intensity of these peaks are different for different occupations of the further-neighbor cation coordination shells. Comparison of Fig. 8(a) with Fig. 8(b)

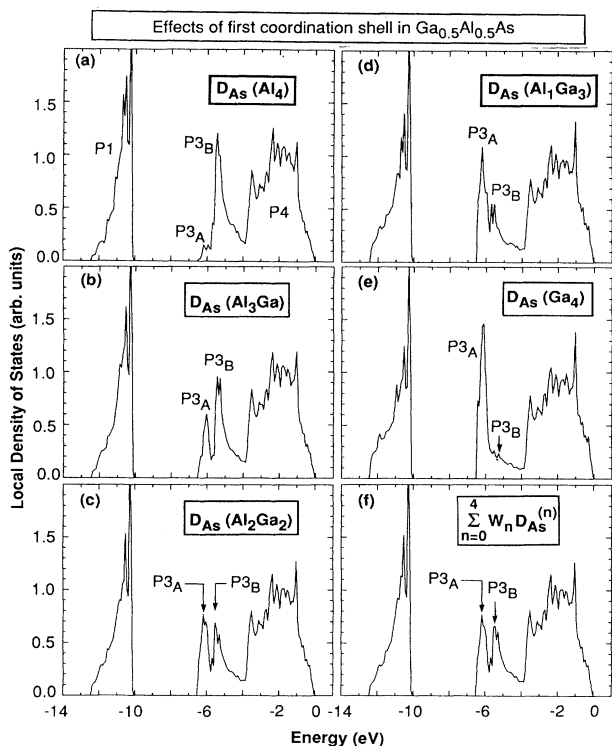


FIG. 7. Decomposition of the total DOS of $\text{Al}_{0.5}\text{Ga}_{0.5}\text{As}$ into As-centered contributions $D_{\text{As}}(\text{Al}_{4-n}\text{Ga}_n)$ associated with the five ($0 \leq n \leq 4$) first-neighbor cation environments [parts (a)–(e)]. Note that the amplitude of $P3_A$ increases as the Al content increases in each cluster, whereas the amplitude of $P3_B$ increases with the Ga concentration in each cluster. Recall that all of these results correspond to a fixed ($x = \frac{1}{2}$) global composition in a homogeneous alloy. Part (f) shows the “average As LDOS” obtained by superposing $\sum_n w_n D_{\text{As}}(\text{Al}_{4-n}\text{Ga}_n)$ with the random tetrahedral probabilities w_n .

shows the effects due to different occupations of the coordination shells beyond the third.

Second-neighbor effects about Al can be discerned by calculating $D_{\text{Al}}(\text{Al}_{12-m}\text{Ga}_m)$ for various m values, depicted in Fig. 9. To focus on the second-neighbor effects, we have averaged, where appropriate, the different occupations of the further coordination shells. In SQS8_a and SQS8_b , only four different occupations of the second coordination shell are present. The trend observed from top to bottom in Fig. 9 (i.e., with increasing number of Al atoms in the second shell) is a decrease in the DOS between the Ga-like and the Al-like $P3$ peaks and an increase in the $P3_B$ intensity at the expense of that of $P3_A$. As the number of Al atoms in the second shell increases, $D_{\text{Al}}(\text{Al}_{12-m}\text{Ga}_m)$ approaches the local Al density of states in the binary AlAs [Fig. 3(d)]. As before, we find that the LDOS of two Al-centered clusters with the same second-shell coordination can still show considerable differences if the occupations of further coordination shells are different.

D. Comparison with experiment

Tsang *et al.*^{47(a)} have recently measured the Al $L_{2,3}$ soft-x-ray emission (SXE) in $\text{Al}_x\text{Ga}_{1-x}\text{As}$, reflecting the Al-centered LDOS. In what follows, we compare our results (Fig. 9) with their data.

(i) Our $P1$ peak energy shows negligible dependence on the number N_{Al} of Al atoms in the first (Fig. 7) and second (Fig. 9) coordination shells. The SXE data^{47(a)} shows, indeed, that this peak (termed there $P3$) does not shift with Al concentration.

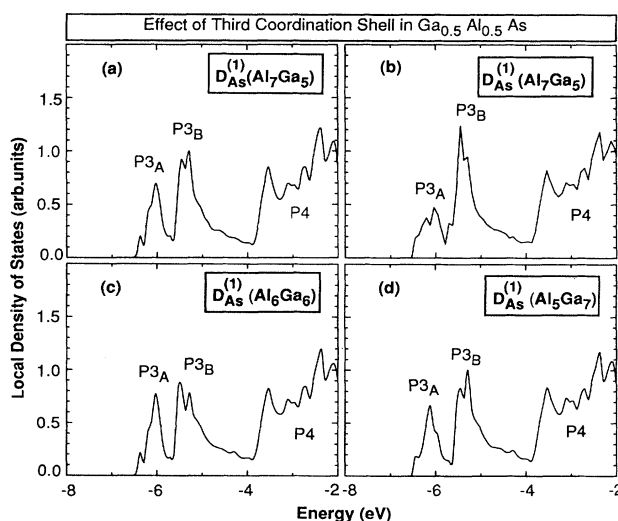


FIG. 8. Decomposition of the $D_{\text{As}}(\text{Al}_3\text{Ga})$ LDOS [Fig. 7(b)] into contributions arising from different occupations of the third $\text{Al}_{12-m}\text{Ga}_m$ shell. Note that parts (a) and (b) have the same occupations through the third coordination shell; the small differences in their DOS reflect effects of more distant shells.

(ii) The calculated $P3$ peak shows a deep, Ga-like component ($P3_A$) and a lower binding-energy Al-like component ($P3_B$). As the number $N_{Al}^{(2)}$ of Al atoms in the second shell about Al increases, the Ga-like peak $P3_A$ narrows (Fig. 9) but the intensity stays nearly constant (although not shown, the same trend is found in the Ga-centered LDOS). On the other hand, the Al-like $P3_B$ peak shows a pronounced increase in intensity (and some narrowing) as $N_{Al}^{(2)}$ increases. While we have not calculated the LDOS at other compositions, we can speculate that the trends with increasing the Al composition x will parallel those of increasing N_{Al} at a fixed x . While the SXE spectra do not resolve $P3_A$ from $P3_B$, they clearly show that as the Al concentration increases, the deeper binding energy part of $P3$ [termed $P2$ in Ref. 47(a)] narrows asymmetrically, while the higher binding-energy

part stays at a similar width but the peak intensity increases significantly. Hence, as x_{Al} increases, there is a transfer of spectral intensity from $P3_A$ to $P3_B$, as seen in our calculation (Fig. 9). This “nonrigid” behavior of $P3$ is the hallmark of this spectral region, found also in other alloys (Sec. VI below). The same trends were seen in a recent tight-binding CPA calculation by Hass.^{47(b)} The measured position of the peak intensity of $P3$ at $x=0.5$ (extrapolated between $x=0.4$ and $x=0.6$) is $E_{vbm}-5.8$ eV, close to our result (average of $P3_A$ and $P3_B$) of $E_{vbm}-(5.8\pm 0.1)$ eV.

(iii) Our $P4$ peak [denoted $P1$ in Ref. 47(a)] shows only weak dependence on $N_{Al}^{(2)}$, in agreement with the fact that its width and intensity do not vary much with x_{Al} .

(iv) Comparison of our results for the pure constituents [Fig. 5(a)] with those of the $x=0.5$ alloy [Fig. 5(c)] and the foregoing analysis of the effects of $N_{Al}^{(2)}$ suggest that while the global composition x changes the energy position of the various peaks, the shape of the peaks is determined primarily by the local environment (N_{Al} and N_{Ga}) in successive shells.

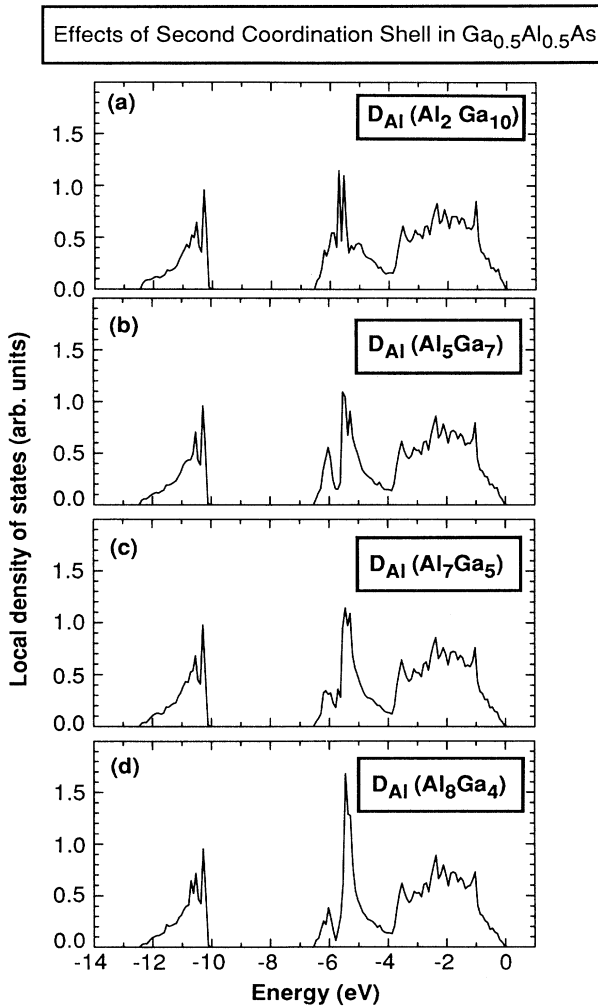


FIG. 9. Decomposition of the Al-centered LDOS into contributions arising from different occupations of the second $Al_{12-m}Ga_m$ shell: (a) (Al_2Ga_{10}) ; (b) (Al_5Ga_7) ; (c) (Al_7Ga_5) ; (d) (Al_8Ga_4) .

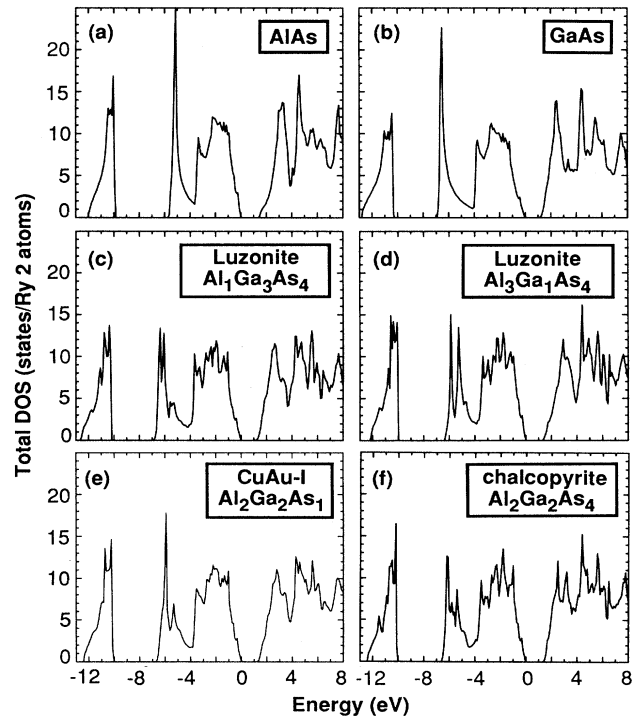


FIG. 10. Total DOS of ordered periodic $Al_nGa_mAs_{n+m}$ structures: (a) and (b) give the results for the binary zinc-blende compounds, (c) gives the DOS of $AlGa_3As_4$ in the luzonite structure, (d) gives the DOS the Al_3GaAs_4 in the luzonite structure, (e) shows the DOS in the CuAu-I-like structure (an $(AlAs)_1(GaAs)_1$ superlattice with layer alternation along the [001] direction), (f) shows the DOS in the chalcopyrite structure (an $(AlAs)_2(GaAs)_2$ superlattice with layer alternation along the [201] direction).

E. Comparison with the method of superposition of periodic structures

It has been suggested previously^{28,29} that the electronic density of states of a random alloy could be modeled by superposing those of a number of ordered structures each containing a distinct repeated cluster. For example, the A_4 or B_4 clusters appear as a repeated motive in the zinc-blende structures AC and BC , respectively, the A_2B_2 cluster appears in the (001) monolayer superlattice $(AC)_1/(BC)_1$ (The CuAu-like structure, or CA), and the A_3B and AB_3 clusters appear in the “Luzonite” structures A_3BC_4 and AB_3C_4 (denoted as $L1$ and $L3$, respectively). To examine this approach we have calculated the DOS of the five *periodic* crystals AC , A_3BC_4 , $A_2B_2C_4$, AB_3C_4 , and BC (Fig. 10) and superposed them using as weights the Bernoulli probabilities appropriate to $x = \frac{1}{2}$. The resulting DOS [Fig. 11(a)] compares reasonably well to that obtained in the more accurate SQS8 model [Fig. 11(b)]. In particular, both models show the splitting of $P3$ structure and the broadening of $P5$ peak. However, we notice from Fig. 10 that the long-range order can substantially modify the “cluster” extracted from these ordered structures. While the *total* DOS obtained by the method of superposition of periodic clusters is rather similar to what is obtained from the SQS, the *partial* DOS can differ. First, note that ordered structures of the same global composition (e.g., CA and CH) differ in their coordination arrangements. For example, relative to an A atom at the origin, the CA structure has 4, 6, 8, 12, 8, 8, and 16 A atoms in shells 1 through 7, respectively, whereas the CH structure has 4, 4, 16, 4, 8, 0, and 32 A

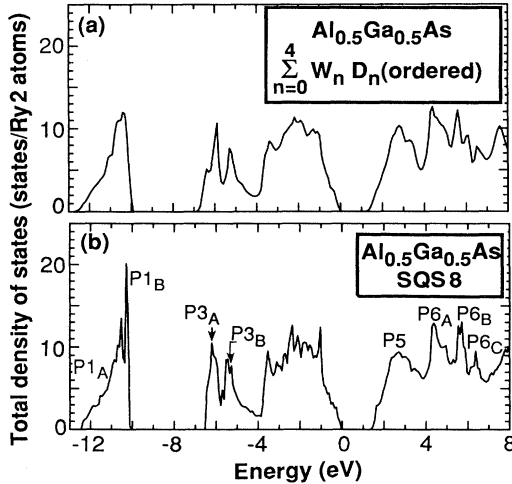


FIG. 11. Comparison of the total DOS of $\text{Al}_{0.5}\text{Ga}_{0.5}\text{As}$ as obtained (a) from averaging SQS8_a and SQS8_b [identical to Fig. 5(c)] with (b) the model of “superposition of periodic structures” [Ref. 29(c)] where the density of states of the five ordered structures $\text{Al}_{4-n}\text{Ga}_n\text{As}_4$ ($0 \leq n \leq 4$) given in Fig. 10 are superposed with random probability weights. [This is distinct from averaging LDOS shown in Fig. 7(f).]

atoms in these respective shells. The DOS of these two crystals are indeed somewhat different: CH has a structure between $P3_A$ and $P3_B$ that CA lacks and the intensity ratios of the various $P1$ subpeaks are different. Clearly, the success of the method of superposition of periodic structures depends on a judicious choice of structures. Second, note that the DOS associated to the clusters in the simple *periodic* structures (Fig. 10) differ from those extracted from the SQS (Fig. 7). For example, the DOS of the AlGa_3 Luzonite cluster [Fig. 10(c)] differs from that in the SQS [Fig. 7(d)] in that $P3_A$ of the former is slightly split. Also, the DOS of the Al_3Ga Luzonite cluster [Fig. 10(d)] differs slightly from that of Fig. 7(b) in the relative $P3_A:P3_B$ intensities.

Finally, note that using a *single* simple (not a SQS) periodic structure to describe the random alloy of the

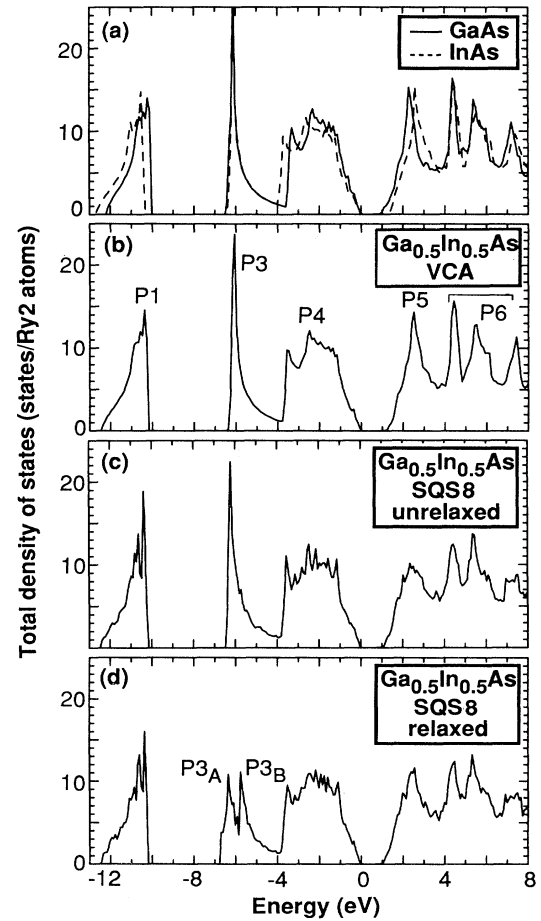


FIG. 12. Total DOS of the GaAs-InAs system. (a) Binaries at the unrelaxed alloy equilibrium lattice constant $\bar{a}_{\text{UR}} = 5.80 \text{ \AA}$, (b) VCA, at the same lattice constant, (c) unrelaxed SQS8 (averaged over variants a and b), and (d) relaxed SQS8 (see Table II for the relaxed bond lengths). The calculated equilibrium lattice constants in SQS8 for fixed and relaxed cell-internal parameters are 5.80 and 5.82 Å , respectively. Note in (c) and (d) the relaxation-independent splitting in the $P1$ region absent in the VCA and the relaxation-induced splitting in the $P3$ region.

same composition can lead to significant errors unless the periodic structure is selected carefully. This has been pointed out by Boguslawski and Baldereschi⁴⁸ who used periodic $\text{Ga}_{4-n}\text{In}_n\text{As}_4$ crystals to describe, for $n=1$ (*L1*), $n=2$ (*CA*), and $n=3$ (*L3*) the $\text{Ga}_x\text{In}_{1-x}\text{As}$ alloy at compositions $x = \frac{3}{4}$, $\frac{1}{2}$, and $\frac{1}{4}$, respectively. The fact that this is not a very good approximation can be also seen by comparing the $n=2$ (*CA*) density of states of Fig. 10(e) with the corresponding SQS results of Fig. 5(c).

VI. RESULTS FOR $\text{Ga}_{0.5}\text{In}_{0.5}\text{As}$ and $\text{GaAs}_{0.5}\text{P}_{0.5}$

Comparison of the density of states of the lattice-mismatched $\text{Ga}_{0.5}\text{In}_{0.5}\text{As}$ and $\text{GaAs}_{0.5}\text{P}_{0.5}$ systems in their unrelaxed and relaxed structures permits analysis of structural disorder effects. Because of the different environment of each atom, structural relaxations lead to a

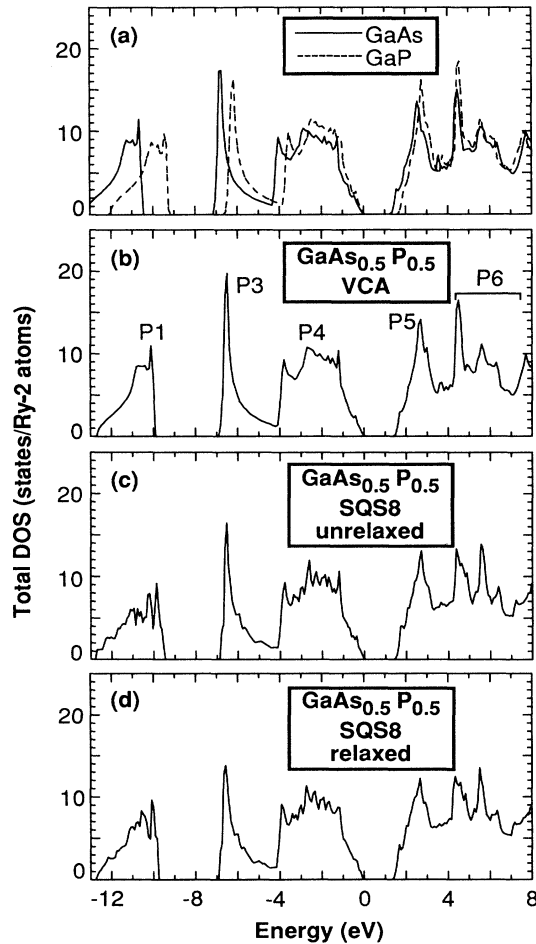


FIG. 13. Total DOS of the GaAs-GaP system. (a) Binaries at the alloy lattice constant $\bar{a}=5.51$ Å, (b) VCA, (c) unrelaxed SQS8 (averaged over the variants *a* and *b*), and (d) relaxed SQS8 (see Table I for the relaxed bond lengths) all at the same lattice constant. Note in (c) and (d) the broadening and splitting in the *P1* region and that the *P3* region remains unsplit in the alloy, unlike the case in GaAs-InAs (Fig. 12).

distribution of bond lengths and angles even in a perfectly random alloy. This feature is included in our calculation by permitting the atoms in the SQS8 to relax into their minimum energy positions. Since all nearest-neighbor A_nB_{4-n} clusters are present in $\text{SQS8}_a + \text{SQS8}_b$, the effects of relaxation on the DOS should mimic realistically the situation in the random alloy. The density of states of $\text{Ga}_{0.5}\text{In}_{0.5}\text{As}$ and $\text{GaAs}_{0.5}\text{P}_{0.5}$ SQS8 are shown in Figs. 12 and 13 where they are compared with the DOS of the binary constituents and of the virtual crystal. In what follows we analyze the behavior of each feature in the DOS.

A. The *P1* region

The *P1* (anion,*s*) region in the SQS of $\text{In}_{0.5}\text{Ga}_{0.5}\text{As}$ exhibits a fine structure with many subpeaks. This behavior is enhanced in the mixed anion system $\text{GaAs}_{0.5}\text{P}_{0.5}$, where two different anion *s* orbitals contribute to this structure.

Since the wave functions associated with the *P1* states are largely *atom-centered* states with nearly spherical

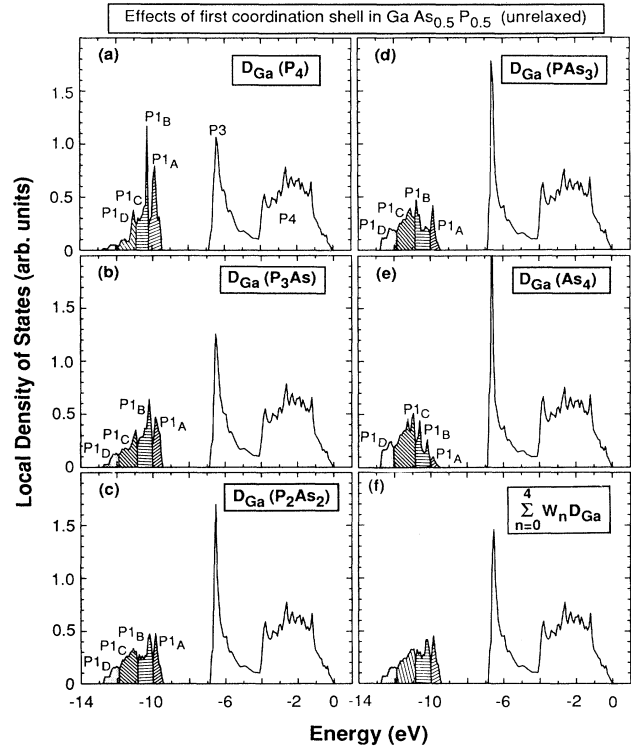


FIG. 14. Decomposition of the total DOS of $\text{GaAs}_{0.5}\text{P}_{0.5}$ into Ga-centered contributions $D_{\text{Ga}}(\text{As}_{4-n}\text{P}_n)$ associated with the five ($0 \leq n \leq 4$) first-neighbor anion environments [parts (a)–(e)]. Note in the *P1* region how the amplitude of the different subpeaks reflects the relative P/As content in each first-neighbor cluster: $P1_A$ and $P1_B$ are reduced in the series $\text{P}_4 \rightarrow \text{P}_3\text{As} \rightarrow \text{P}_2\text{As}_2 \rightarrow \text{PAs}_3 \rightarrow \text{As}_4$ whereas $P1_C$ and $P1_D$ increase as the As content increases in each cluster. Part (f) shows the “average Ga LDOS” obtained by superposing $D_{\text{Ga}}(\text{P}_{4-n}\text{As}_n)$ with the random tetrahedral probabilities.

symmetry about the anion sites [see Fig. 2(a)], the energy levels in this region are not perturbed severely by relaxing the bond lengths and angles at a fixed volume. Like in $\text{Al}_{0.5}\text{Ga}_{0.5}\text{As}$, the splitting and broadening in the $P1$ region of $\text{In}_{0.5}\text{Ga}_{0.5}\text{As}$ can be traced back to the existence of structurally inequivalent As atoms. In $\text{GaAs}_{0.5}\text{P}_{0.5}$ the $P1$ region shows a greater complexity, because of the mixing between the P and As s levels. Moreover, it shows some changes on passing from the unrelaxed to the relaxed structure. We have analyzed the contribution of the five nearest-neighbor clusters on the local density of states on Ga atoms. The results are displayed for unrelaxed $\text{GaAs}_{0.5}\text{P}_{0.5}$ in Fig. 14. The amplitudes of the different $P1$ subpeaks change following the cluster sequence $P_4 \rightarrow P_3\text{As}_2 \rightarrow P\text{As}_3 \rightarrow \text{As}_4$. The amplitude of the peak $P1_A$ at about $E_v - 9.9$ eV decreases as the P content of the cluster diminishes. Examination of the charge density in this energy region [shown in Fig. 15(a)], reveals that this feature is associated with states having s -like symmetry around the P atoms, just like in pure GaP. In this energy region there is no mixing between P and As s orbitals. On the other hand, the feature $P1_D$ at about $E_v - 12.3$ eV (Fig. 14) grows in going from the cluster P_4 to the cluster As_4 . Inspection of the associated charge density in Fig. 15(d) shows that this structure is related mostly to s orbitals on the As atoms. The regions $P1_B$

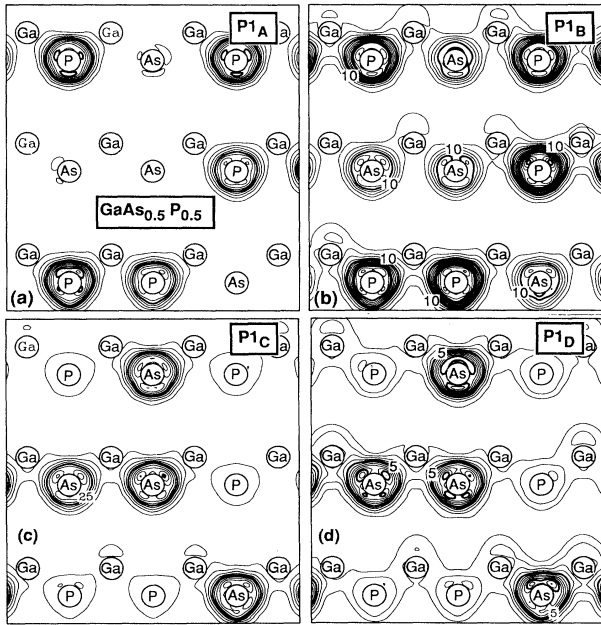


FIG. 15. Electronic charge density contours in the (110) plane for the unrelaxed $\text{GaAs}_{0.5}\text{P}_{0.5}$ SQS8 in the $P1$ region. (a) $P1_A$ at $E_v - 9.5$ eV to $E_v - 10.0$ eV; (b) $P1_B$ at $E_v - 10.0$ eV to $E_v - 10.9$ eV; (c) $P1_C$ at $E_v - 10.9$ eV to $E_v - 12.0$ eV; (d) $P1_D$ at $E_v - 12.0$ eV to $E_v - 13.0$ eV. $P1_A$ and $P1_B$ are predominantly P-centered states, while $P1_C$ and $P1_D$ are predominantly As-centered states. The contour steps for parts (a)–(d) are, respectively, 2.5, 2.5, 5.1 (in units of electrons per unit cell volume).

and $P1_C$ between $E_v - 10$ eV and $E_v - 11.8$ eV show the most pronounced changes on passing from one cluster to another (Fig. 14). The charge densities of these structures are plotted in Figs. 15(b) and 15(c), respectively. We see from Fig. 15(b) that the wave functions associated with the region $P1_B$ are mostly centered around the phosphorus atoms, with a considerable probability also around the As atoms. From Fig. 15(c) we deduce that the $P1_C$ state, extending from about $E_v - 11$ eV to higher binding energies, is As, s like with mixing of amplitude on the P atoms. From this analysis we can divide the $P1$ peak into three regions: (i) an As, s like region ($P1_D$ and a large part of $P1_C$) from about $E_v - 11$ eV to $E_v - 12.8$ eV, (ii) a P, s like region ($P1_A$) from $E_v - 9.5$ eV to about $E_v - 10$ eV, and (iii) an intermediate region where the wave functions are extended on both As and P atoms. This is confirmed by the comparison with the DOS of relaxed $\text{GaAs}_{0.5}\text{P}_{0.5}$, Fig. 13(d), where we see that the largest change in the shape of $P1$ with respect to the unre-

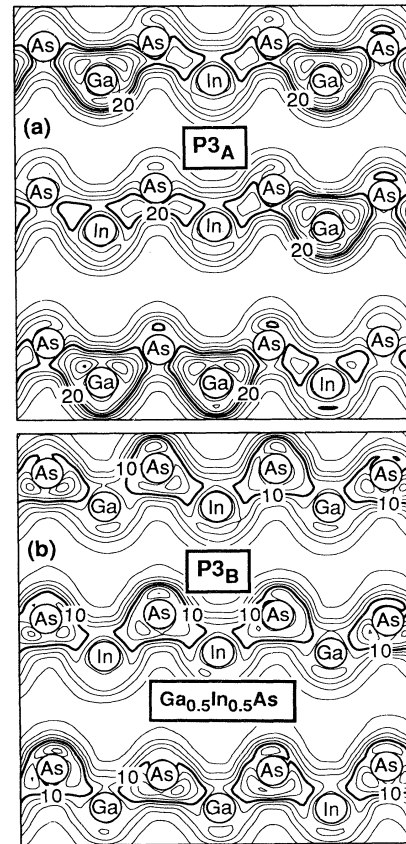


FIG. 16. Electronic charge density contours in the (110) plane for the relaxed $\text{In}_{0.5}\text{Ga}_{0.5}\text{As}$ SQS8 in the $P3$ region. (a) $P3_A$ from $E_v - 6.9$ eV to $E_v - 5.9$ eV; (b) $P3_B$ from $E_v - 5.9$ eV to $E_v - 4.0$ eV. $P3_A$ is mostly centered on the Ga—As bonds while $P3_B$ on the In—As bond. The contour steps for parts (a) and (b) are, respectively, 4 and 2 (in units of electrons per unit cell volume).

laxed case occurs just in this energy region. These mixed states are the most sensitive to the structural relaxation. We notice, moreover a change in the energy onset of $P1_A$ peak with relaxation, reflecting the shift of the $P1$ peak in GaP to higher binding energies with volume compressing (bond shortening).

B. The $P3$ and $P5$ regions

Unlike the atom-centered $P1$ states, the bonding and antibonding $P3$ and $P5$ states have directional character, and are hence expected to respond more strongly to constant-volume bond relaxations. Figure 16 depicts the charge density in the $P3$ region of $\text{Ga}_{0.5}\text{In}_{0.5}\text{As}$, and shows that the deeper binding-energy $P3_A$ component is constructed predominantly from Ga-As states, whereas the lower binding energy $P3_B$ component has more weight on the In-As bond. The behavior of the $P3$ peaks both in $\text{In}_{0.5}\text{Ga}_{0.5}\text{As}$ and in $\text{GaAs}_{0.5}\text{P}_{0.5}$ is particularly interesting, in that the $P3$ energies of the pure *binary* constituents at the alloy's equilibrium volume are nearly degenerate in GaAs and InAs [Fig. 12(a) and Table II], whereas in GaAs and GaP the $P3$ energy separation is significant [Fig. 13(a) and Table II]. However, we see from Figs. 12 and 13 that alloy relaxation *induces* a splitting in the $P3$ region of $\text{Ga}_{0.5}\text{In}_{0.5}\text{As}$, whereas in $\text{GaAs}_{0.5}\text{P}_{0.5}$ the alloy environment acts to *remove* the initial $P3$ splitting. Similar effects were noticed and analyzed in II-VI alloys.³²

This behavior is caused by two effects. (i) While in AlAs and GaAs each As is coordinated, respectively, by Al_4 and Ga_4 , leading to a maximal difference in the positions of the respective $P3$ peaks (Appendix), in the alloy there are also mixed Al-Ga clusters that fill in additional DOS features between the Al_4 and Ga_4 peaks. Indeed, Fig. 16 shows that in $\text{In}_{0.5}\text{Ga}_{0.5}\text{As}$ the $P3_A$ peak involves In-As minority character whereas the $P3_B$ peak involves Ga-As minority character. The same is true in $\text{GaAs}_{0.5}\text{P}_{0.5}$, where the 0.6-eV $P3$ splitting in the binaries (Table II) is reduced [Fig. 13(c)] by hybridization. (ii) Bond relaxation further modifies these states. To understand this different behavior we have schematically plotted in Fig. 17 the shifts in the sp^3 bonding ($P3$) and antibonding ($P5$) states due to relaxations. Previous calculations^{32,41,44} have shown that bonding (antibonding) states are displaced to larger (smaller) binding energies when the bond lengths are shortened. Our calculation showed (Table I) that upon relaxation of $\text{In}_{0.5}\text{Ga}_{0.5}\text{As}$, the In-As bond becomes longer, while the Ga-As bond becomes shorter relative to the unrelaxed virtual lattice average. These changes are denoted in Fig. 17 by the arrows. As a consequence, the In-As bonding $P3_B$ component shifts to lower binding energies while the Ga-As $P3_A$ component shifts to deeper binding energies [Fig. 17(b)]. Thus, relaxation *increases* the $P3_A$ - $P3_B$ separation in $\text{In}_{0.5}\text{Ga}_{0.5}\text{As}$, as observed in Figs. 12(c) and 12(d). The opposite is true for the antibonding $P5$ peak in $\text{In}_{0.5}\text{Ga}_{0.5}\text{As}$, where relaxation tends to bring the peaks closer [Fig. 17(a)]. In $\text{GaAs}_{0.5}\text{P}_{0.5}$ relaxation elongates the Ga-As bond while the Ga-P bond becomes short-

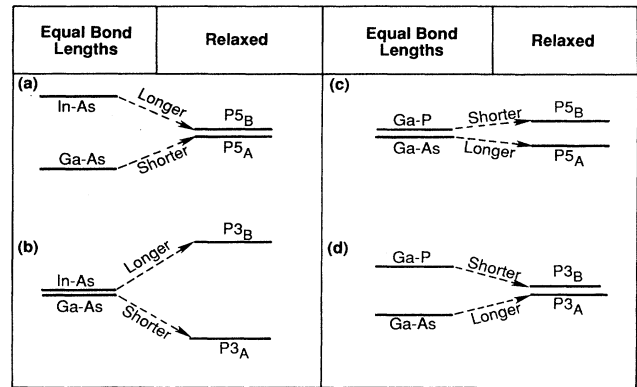


FIG. 17. Schematic plot of the effects of bond relaxation on the energies of the bonding $P3$ and antibonding $P5$ states in the $\text{Ga}_{0.5}\text{In}_{0.5}\text{As}$ [parts (a) and (b)] and $\text{GaAs}_{0.5}\text{P}_{0.5}$ [parts (c) and (d)] alloys. “Longer” and “shorter” refer to changes in the bond lengths relative to the equal $A-C$ and $B-C$ bond lengths in the unrelaxed alloys (denoted VLA in Table I).

er. Hence, the higher binding energy Ga-As $P3_A$ states shift upon relaxation to a lower binding energy, while the Ga-P component $P3_B$ shifts to higher binding energy [Fig. 17(d)]. Thus, relaxation *reduces* the energy-level separation between the two $P3$ components in $\text{GaAs}_{0.5}\text{P}_{0.5}$. The opposite is true for the $P5$ peak [Fig. 17(c)]. Since the splittings are rather small in $\text{GaAs}_{0.5}\text{P}_{0.5}$, the changes with relaxation are not apparent in Fig. 13.

C. The $P4$ and $P6$ regions

Like in $\text{Al}_{0.5}\text{Ga}_{0.5}\text{As}$, the $P4$ region shows a fine structure in the SQS model. These features are very similar in both the common-anion and the common-cation alloys and change relatively little with relaxation. The $P6$ region shows broadening for both systems. In $\text{GaAs}_{0.5}\text{P}_{0.5}$ we can notice a splitting of the lower binding-energy component as already seen in $\text{Al}_{0.5}\text{Ga}_{0.5}\text{As}$.

VII. COMPARISON WITH PREVIOUS DOS CALCULATIONS

Lempert and co-workers¹⁹ have calculated the DOS of $\text{In}_{0.5}\text{Ga}_{0.5}\text{As}$ in three different alloy models: (a) VCA, where chemical and structural disorder are both neglected, (b) site CPA, where only the chemical disorder has been introduced, and (c) MCPA, where both kinds of disorder were taken into account. Comparing SCPA with VCA (Fig. 18) they found that the introduction of chemical disorder broadens the peaks $P3$ and $P5$, leaving the structures $P1$ and $P4$ in the valence band substantially unchanged. Similar results are obtained here in passing from the VCA [Fig. 12(b)] to the unrelaxed SQS [Fig. 12(c)], except that we find distinctly new fine structures in $P1$ and $P4$. Comparing the MCPA to the SCPA, Lem-

pert and co-workers find that the introduction of the structural disorder tends to increase the broadening throughout the upper valence bands. They observed the presence of two bumps in the $P3$ peak, analogous to $P3_A$ and $P3_B$ found here [compare Fig. 12(c) with Fig. 12(d)], except that the splitting found here is considerably larger. Another feature related to the introduction of the structural relaxation in their model is the decrease of broadening of the $P5$ peak relative to the site-CPA model analogous to the present results. Hence, the MCPA calculations capture the overall shape (but not the details) found in SQS models.

All other existing calculations on III-V semiconductor alloy DOS are restricted to the VCA and SCPA. The most detailed are the CPA calculation of Chen and Sher¹⁸ on $\text{GaP}_{0.5}\text{As}_{0.5}$ and on $\text{Ga}_{0.5}\text{In}_{0.5}\text{As}$. For $\text{Ga}_{0.5}\text{In}_{0.5}\text{As}$ (where the scattering strength is largest), they find [Fig. 19(a)] that the CPA density of states represents a mere broadening of the valence-band structures with respect to the VCA. In conflict with Lempert and co-workers¹⁹ their $P1$ and $P4$ peaks show CPA-induced broadening. The fine structure in $P1$ and $P4$ (Fig. 12) and relaxation effects are all missed by this calculation. The results for $\text{GaP}_{0.5}\text{As}_{0.5}$ [Fig. 19(b)] show essentially the same valence-band features in the scaled VCA and CPA models. Only for the first conduction bands does the CPA show a slight broadening of the peaks. Our results on $\text{GaP}_{0.5}\text{As}_{0.5}$ system (Fig. 13) show instead a pronounced broadening of the structures, in particular $P3$, $P5$, and $P6$ on passing from the VCA model to the unrelaxed SQS8. In particular the $P1$ structure is the most affected by the introduction of the chemical disorder. For the

lattice-matched $\text{Al}_x\text{Ga}_{1-x}\text{As}$ system, the present results are very similar to the CPA results of Hass.^{47(b)}

VIII. BOWING OF THE DIRECT OPTICAL BAND GAPS

We have calculated the direct band gaps at Γ in the SQS8 model for the three systems. Table III gives the energies at the top of the valence band and the energy of the conduction state of Γ_{1c} character. The crystal-field splitting at the top of the valence band is enhanced by relaxation. Table IV gives the calculated optical bowing coefficient for the three systems together with their decompositions in chemical and structural contributions. The bowing coefficient is defined as four times the difference between the average band gap of the two binary constituents and the band gap (relative to the average of the crystal-field components at VBM) of the SQS alloy. The “volume deformation” is defined as the contribution due to the compression and/or dilation of the binary constituents into the alloy’s volume \bar{V} . The “charge exchange” is defined as the change in going from the binaries at \bar{V} to the unrelaxed SQS, while the “structural relaxation” is the change in passing from the unrelaxed to the relaxed SQS. The contributions from volume deformation (VD) and structural relaxation (SR) are present only for lattice-mismatched systems. We notice that the chemical exchange (CE) contribution is small and negative for both lattice-mismatched systems, while it is positive and larger for $\text{Al}_{0.5}\text{Ga}_{0.5}\text{As}$ having the greatest mismatch in atomic orbital energies.⁴³ This is consistent with the observation that the effect of compo-

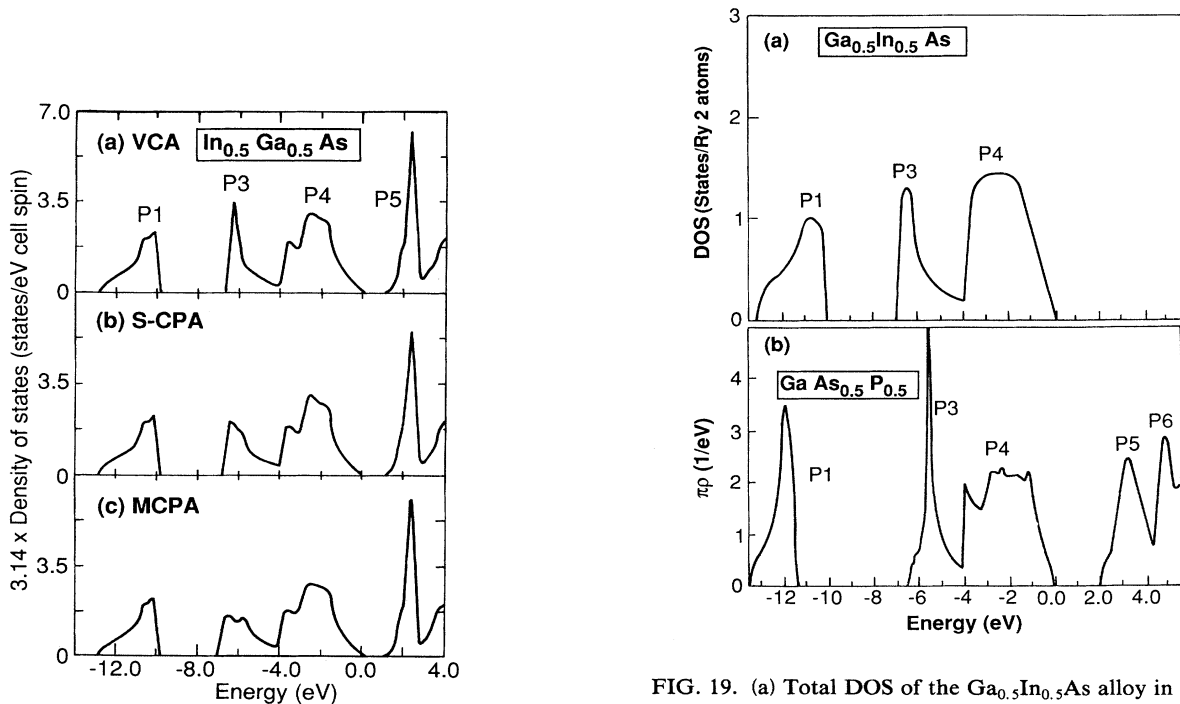


FIG. 18. Total DOS of the $\text{In}_{0.5}\text{Ga}_{0.5}\text{As}$ alloy in the (a) VCA, (b) site CPA, and (c) MCPA from Ref. 19.

FIG. 19. (a) Total DOS of the $\text{Ga}_{0.5}\text{In}_{0.5}\text{As}$ alloy in the CPA from Ref. 18 [Chen and Sher, Phys. Rev. B **17**, 4726 (1978)]; (b) total DOS of the $\text{GaAs}_{0.5}\text{P}_{0.5}$ alloy in the CPA from Ref. 18 [Chen and Sher, Phys. Rev. B **23**, 5360 (1981)].

sitional disorder is larger in lattice-matched systems.⁴⁹ Structural relaxation contributes in a different way to the bowing of GaAs_{0.5}P_{0.5} and Ga_{0.5}In_{0.5}As. To explain this different behavior we notice that the top of the valence band in Ga_{0.5}In_{0.5}As has more In than Ga character (see also the Appendix), while the bottom of the conduction band has more Ga than In character. Structural relaxation increases the In—As bond lengths thereby raising the energy of the bonding valence-band maximum (VBM), while the reduction in the Ga—As bond lengths raises the energy of the antibonding states at the conduction-band minimum (CBM). The net effect is a slight increase of the direct band gap with respect to the unrelaxed configuration. In GaAs_{0.5}P_{0.5}, on the other hand, both the VBM and the lowest conduction state at Γ have more As than P character. Since structural relaxation increases the Ga—As bond lengths, this reduces the band gap giving a positive contribution to the band bowing. In all cases the total bowing $b = b_{VD} + b_{CE} + b_{SR}$ is positive, leading to a reduction of the direct band gap. The reduction is biggest for Ga_{0.5}In_{0.5}As that presents the largest lattice mismatch. Neglect of relaxation leads to an underestimation of the bowing coefficient of about 42% in GaAs_{0.5}P_{0.5} and to its overestimation of about 18% in Ga_{0.5}In_{0.5}As.

In the case of Ga_{0.5}In_{0.5}As and Al_{0.5}Ga_{0.5}As random alloys there is a substantial spread in the experimental optical bowing parameters. The reported values range between 0.32 and 0.61 eV for Ga_{0.5}In_{0.5}As (Ref. 50) and between 0 and 0.37 eV for Al_{0.5}Ga_{0.5}As.⁵¹ For Ga_{0.5}Al_{0.5}As the most recent determination of the direct gap bowing by Bosio *et al.*⁵² gives the value (0.22±0.06) eV in very good agreement with our calculated value of

0.20 eV. For the GaInAs alloy, lattice matched to InP (0.44 < x < 0.49), Goetz *et al.*⁵³ give the value $b = 0.475$ eV, close to our calculated value of 0.40 eV. Also for GaAs_{0.5}P_{0.5} there is a good agreement between the various experimental values $b_{\text{expt}} = 0.17\text{--}0.21$ eV (Ref. 54) and our calculated total optical band bowing of 0.19 eV.

The spread of calculated values is even bigger. The bowing calculated here for Ga_{0.5}In_{0.5}As using the SQS8 model in the pseudopotential approach (0.40 eV) is in very good agreement with our previously calculated linearized-augmented-plane-wave value for SQS4 of 0.43 eV.^{29(b)} Lempert and co-workers¹⁹ have found that the introduction of the structural disorder in Ga_{0.5}In_{0.5}As through the MCPA model reduces the optical bowing. They give the following values: $b_{VCA} = 0.24$ eV, $b_{CPA} = 0.32$ eV, and $b_{MCPA} = 0.26$ eV. Baldereschi and Maschke,⁵⁵ using the pseudopotential method and second-order perturbation theory on GaP _{x} As _{$1-x$} , found $b \approx 0.27$ eV. Lee *et al.*,⁵⁶ using a modified empirical tight-binding method, calculated $b \approx 0.74$ eV for Ga _{$1-x$} In _{x} As. Both studies conclude that structural relaxation (not included in their model) has almost a negligible effect on the direct band gap bowing, the main contribution coming from the compositional disorder. This is in disagreement with our findings, where the structural effects are very important (Table IV), mostly for the GaAs_{0.5}P_{0.5} alloy, and the compositional disorder (CE) has little effect in lattice-mismatched systems.

We conclude with a note on the different b_{VCA} values obtained here for the three alloys. In the literature one finds different values for the direct gap optical bowing of the GaAs _{$1-x$} virtual crystal. Ting and Chang,⁵⁷ using an empirical $k \cdot p$ method to calculate the band structure,

TABLE III. Calculated energies (in eV) of the Γ_{15v} and Γ_{1c} electronic states relative to the top of the valence band for the unrelaxed (UR) and the relaxed (R) SQS8 and the virtual crystal. For SQS8 we give the crystal-field components of the Γ_{15v} state. The energy levels are compared with the average of the energies of the corresponding states in the binary compounds at their equilibrium lattice constant a_{eq} and with those at the alloy lattice constant \bar{a} .

Electronic level	Average energy of binaries at a_{eq}	Average energy of binaries at \bar{a}	SQS8 energy UR at \bar{a}	SQS8 energy R at \bar{a}	VCA energy at \bar{a}
GaAs _{0.5} P _{0.5} ^a					
Γ_{15v}	0.000	0.000	$\begin{cases} -0.009 \\ -0.006 \\ 0.000 \end{cases}$	$\begin{cases} -0.061 \\ -0.049 \\ 0.000 \end{cases}$	0.000
Γ_{1c}	1.443	1.412	1.410	1.358	1.367
Al _{0.5} Ga _{0.5} As ^b					
Γ_{15v}	0.000	0.000	$\begin{cases} -0.014 \\ -0.005 \\ 0.000 \end{cases}$		0.000
Γ_{1c}	1.433	1.433	1.376		1.436
Ga _{0.5} In _{0.5} As ^c					
Γ_{15v}	0.000	0.000	$\begin{cases} -0.005 \\ -0.004 \\ 0.000 \end{cases}$	$\begin{cases} -0.080 \\ -0.069 \\ 0.000 \end{cases}$	0.000
Γ_{1c}	0.261	0.133	0.140	0.116	0.256

^aFor GaAs_{0.5}P_{0.5} we use the alloy value $\bar{a} = 5.51$ Å.

^bFor Ga_{0.5}Al_{0.5}As we use the alloy value $\bar{a} = 5.619$ Å.

^cFor Ga_{0.5}In_{0.5}As we use the alloy value $\bar{a} = 5.818$ Å.

TABLE IV. Decomposition of the direct gap optical bowing coefficient b for SQS8 (using the crystal-field average of the states at the VBM) into “volume deformation” (VD), “charge exchange” (CE), and “structural relaxation” (SR) contributions. The corresponding optical bowing coefficient of the virtual crystal (b_{VCA}) and experimental values are given for comparison. Note that the SQS model gives bowing effects due to only short-range interactions.

	GaAs _{0.5} P _{0.5}	Ga _{0.5} Al _{0.5} As	Ga _{0.5} In _{0.5} As
b_{VD}	+0.12	0.00	+0.51
b_{CE}	-0.01	+0.20	-0.04
b_{SR}	+0.08	0.00	-0.07
b	+0.19	+0.20	+0.40
b_{expt}	0.17–0.21 ^a	0.0–0.37 ^b	0.32–0.61 ^c
b_{VCA}	+0.30	-0.01	+0.02

^aReference 54.

^bReferences 51 and 52.

^cReferences 50 and 53.

find a *negative* bowing ($b \sim -0.56$ eV). The virtual-crystal approximation of Chen and Sher,⁵⁸ who used a tight-binding model for the wave functions and empirical pseudopotentials, gives a *positive* bowing coefficient $b = +0.10$ eV. As indicated by Bernard and Zunger^{29(c)} different VCA calculations within empirical methods can lead to a large spread in predictions even though the underlying fits to the band structures of the pure constituents are equally good. These values are seen to strongly depend on the theoretical method. As recognized by others^{13,16} the VCA is not a viable approach for estimating alloy bowing.

IX. SUMMARY

We have calculated the electronic properties of the random III-V semiconductor alloys Al_{0.5}Ga_{0.5}As, Ga_{0.5}In_{0.5}As, and GaAs_{0.5}P_{0.5} focusing on the effects of chemical and structural disorder. In a random alloy there exists a distribution of many distinct local configurations. Chemically identical atoms contribute differently to the alloy properties if their “local environments” are different. In this work we have analyzed how the electronic properties of semiconductor alloys depend on the average atomic arrangements around sites. The use of the special quasirandom structures approach³⁰ permits a study of the interactions between these different atomic local environments and the global properties of the alloy in that each atom retains its identity.

Aligning the peaks of the density of states (Table II) of two semiconductors on an absolute energy scale (Appendix) reveals differences in the positions of corresponding DOS features. Compressing and dilating these semiconductors to the alloy volume \bar{V} further shifts these peaks due to hydrostatic effects (Fig. 4), producing the “unmixed” states of the constituents. Creating the unrelaxed random alloy at \bar{V} presents chemically identical atoms with different local environments. This leads to coupling

of the “unmixed” states of the constituents, most apparent by the appearance of splittings in the $P1$ anion s states [Figs. 5(c), 12(c), 13(c)] and fine structure in the bonding $P4$ and antibonding $P5$ bands. These features can be traced to a superposition of the various nearest-neighbor local environments about the common atom (Figs. 7 and 14), as well as to second-shell (Fig. 9) and even third-shell (Fig. 8) effects. The SQS construct provides a direct way for inspecting such “superposition effects” and depicting the electronic charge density of various states in real space (Figs. 6, 15, and 16). Relaxation of the atomic positions leads to “bond alternations” whereby the shorter of the two ($A-C$ and $B-C$) binary bonds become yet shorter relative to the virtual lattice average, whereas the longer of the two becomes yet longer in quantitative agreement with EXAFS measurements (Table I). Such nonhydrostatic deformations couple to the electronic states (Fig. 17), enhancing (reducing) the $P3_A-P3_B$ splitting in In_{0.5}Ga_{0.5}As (GaAs_{0.5}P_{0.5}) and reducing (enhancing) the $P5_A-P5_B$ splittings in In_{0.5}Ga_{0.5}As (GaAs_{0.5}P_{0.5}). These structural relaxations contribute significantly to the bowing of the direct band gaps in lattice-mismatched alloys (Table IV).

Our results are qualitatively similar to those obtained by the molecular CPA, where distinct (nearest-neighbor¹⁹) environmental effects are retained, and to the analysis of Gonis, Butler, and Stocks^{21(b)} of environmental effects in metallic alloys. Since, however, the single-site CPA averages out at the outset all environments about single sites, the multisite nature of chemical disorder is lost, as are all relaxation effects. These effects are shown to be significant for size-mismatched semiconductor alloys. While they can be captured by the MCPA, the complexity of this method has so far hindered applications in the context of self-consistent first-principles approaches. We find here, however, that the method of “superposition of periodic structures”^{28,29} (that can be readily implemented in the context of first-principles approaches) captures closely (Figs. 10 and 11) most of the details of chemical and relaxation disorder effects. The results of the SQS method await experimental testing.

ACKNOWLEDGMENTS

We thank S.-H. Wei for helpful discussions and K. C. Hass for valuable comments on the manuscript. This work was supported by the Office of Energy Research, Basic Energy Science (OER-BES), Division of Materials Research, under Grant No. DE-AC02-77-CH00178.

APPENDIX; TRENDS IN DOS PEAK ENERGIES IN III-V COMPOUNDS

These trends can be understood qualitatively in terms of the pertinent atomic orbital energies⁴³ by realizing that these are given on an absolute energy scale, while those of Table II need to be shifted by the relative band offsets to be on an absolute energy scale.

(i) Table II shows that relative to the respective valence-band maxima, $P3(\text{GaAs})$ is 1.4 eV deeper than $P3(\text{AlAs})$, whereas $P1(\text{GaAs})$ is about 0.4 eV deeper than

$P1(\text{AlAs})$. Notice that $P3$ constitute mainly cation s and anion p states while $P1$ is mainly anion s states (with a small amount of cation s). On an absolute energy scale the VBM of AlAs is 0.4–0.5 eV deeper than that of⁴ GaAs. Shifting the AlAs DOS to deeper binding energies by this amount shows that $P3(\text{GaAs})$ is ~ 1 eV deeper than $P3(\text{AlAs})$ whereas the two $P1$ states are approximately degenerate. This follows the trends in the atomic orbital energies:⁴³ the Ga, s orbital is ~ 1.2 eV deeper than Al, s .

(ii) Relative to the VBM, $P1(\text{GaAs})$ is 0.8 eV deeper than $P1(\text{GaP})$, when both constituents are taken at their equilibrium lattice constants, a_{eq} . On an absolute scale, the VBM of GaP is ~ 0.4 eV deeper than that of GaAs (Ref. 45) (both at the alloy intermediate lattice parameter a_{alloy}), so on this scale $P1(\text{GaAs})$ is only ~ 0.4 eV deeper than $P1(\text{GaP})$. This is consistent with the fact that the atomic s orbital energy⁴³ of As is ~ 0.7 eV deeper than that of P and that GaP has shorter bond length, so its bonding states have lower energies. $P3(\text{GaAs})$ is ~ 0.1 eV deeper than $P3(\text{GaP})$ when both are measured with respect to their valence-band maxima at a_{eq} . On an absolute scale the difference is 0.3 eV, GaP being now deeper. Indeed, the P p atomic orbital energy⁴³ is ~ 0.3 eV deeper

than that of As. At a_{alloy} , however, $P3(\text{GaAs})$ deepens by 0.3 eV and $P3(\text{GaP})$ becomes shallower by 0.2 eV, so these hydrostatic effects reverse again the $P3$ energy order.

(iii) Relative to the VBM, $P3(\text{GaAs})$ is 0.9 eV deeper than $P3(\text{InAs})$ while $P1(\text{GaAs})$ is 0.3 eV deeper than $P1(\text{InAs})$ when both constituents are taken at their a_{eq} values. The band offset between GaAs/InAs is only⁴⁴ ~ 0.2 eV, so on an absolute scale the $P3$ difference is increased to 1.1 eV whereas the $P1$ difference is about 0.5 eV. Indeed, the Ga s orbital energy is 0.7 eV deeper than that of In, and GaAs having shorter bond lengths, has lower bonding energies. However, at a_{alloy} the $P3$ energy difference in the solid is diminished to near zero, whereas the $P1$ difference is 0.3 eV, with InAs having lower energy. This reflects the fact that dilation of GaAs reduces the binding energies of its $P1$ and $P3$ states, whereas compression of InAs increases the binding energies of its bonding states (Fig. 4 and Table II). This reverses the trends seen at a_{eq} .

In summary, we see that the trends in the bonding-state energy levels can be explained semiquantitatively on the basis of their initial atomic values and a tight-binding description of the binary compounds.

¹M. B. Panish and M. Ilegems, *Prog. Solid State Chem.* **7**, 34 (1972).

²J. G. Woolley, in *Compound Semiconductors*, edited by R. K. Willardson and H. L. Goering (Reinhold, New York, 1962), p. 3.

³K. J. Bachmann, F. A. Thiel, and H. Schreiber, *Prog. Cryst. Growth Character.* **2**, 171 (1979).

⁴Short-range clustering in disordered semiconductor alloys have been observed in diffraction studies, e.g., J. P. Goweis, *Appl. Phys. A* **31**, 23 (1983); A. G. Norman and G. R. Booker, in *Microscopic Semiconductor Materials*, edited by A. G. Cullis and D. B. Holt, IOP Conf. Proc. No. 76 (Institute of Physics and Physical Society, London, 1985), p. 257; P. E. Brunemeir, T. J. Roth, N. Holonyak, and G. E. Stillman, *Appl. Phys. Lett.* **43**, 373 (1983); P. M. Petroff, A. Y. Cho, F. K. Reinhart, A. C. Gossard, and W. Wiegmann, *Phys. Rev. Lett.* **48**, 170 (1982); C. Bocchi, P. Franzosi, and C. Ghezzi, *J. Appl. Phys.* **57**, 4533 (1985). Random alloys were seen by, e.g., Y. Kashihara, N. Kashiwagura, M. Sakata, J. Harada, and T. Arii, *Jpn. J. Appl. Phys.* **23**, L901 (1984).

⁵K. Beshah, D. Zamir, P. Becla, P. A. Wolff, and R. G. Griffin, *Phys. Rev. B* **36**, 6420 (1987); D. B. Zax, S. Vega, N. Yellin, and D. Zamir, *Chem. Phys. Lett.* **130**, 105 (1987).

⁶I. Sela, V. V. Gridin, R. Besserman, and H. Morkoc, *Phys. Rev. B* **39**, 3254 (1989).

⁷J. C. Mikkelsen and J. B. Boyce, *Phys. Rev. Lett.* **49**, 1412 (1982); *Phys. Rev. B* **28**, 7130 (1983).

⁸N. Motta, A. Balzarotti, P. Letardi, A. Kisiel, M. T. Czyzyk, M. Zimmel-Starnawska, and M. Podgorny, *Solid State Commun.* **53**, 509 (1985); M. T. Czyzyk, M. Podgorny, A. Balzarotti, P. Letardi, N. Motta, A. Kisiel, and M. Zimmel-Starnawska, *Z. Phys. B* **62**, 153 (1986); M. Ichimura and A. Sasaki, *J. Appl. Phys.* **60**, 3850 (1986).

⁹(a) T. Sasaki, T. Onda, and R. Ito, *Jpn. J. Appl. Phys.* **25**, 231 (1986); (b) J. Bellessa, C. Gors, P. Launois, M. Quillec, and H. Launois, in *International Symposium on GaAs and Related*

Compounds, Albuquerque, 1982, edited by G. Stillman, IOP Conf. Proc. No. 65 (Institute of Physics and Physical Society, London, 1983), Chap. 6, p. 529.

¹⁰T. S. Kuan, T. F. Kuech, W. I. Wang, and E. L. Wilkie, *Phys. Rev. Lett.* **54**, 201 (1985); H. R. Jen, M. J. Cherng, and G. B. Stringfellow, *Appl. Phys. Lett.* **48**, 1603 (1986); A. Gomyo, T. Suzuki, and S. Iijima, *Phys. Rev. Lett.* **60**, 2645 (1988).

¹¹See a recent review on theories of metal alloys by G. M. Stocks and H. Winter, in *The Electronic Structure of Complex systems*, edited by P. Phariseau and W. M. Temmerman (Plenum, New York, 1984), p. 463.

¹²J. S. Faulkner, *Prog. Mater. Sci.* **27**, 1 (1982).

¹³See a recent review on theories of electronic structure of semiconductor alloys by M. Jaros, *Rep. Prog. Phys.* **48**, 1091 (1985).

¹⁴R. Magri, S.-H. Wei, and A. Zunger, *Phys. Rev. B* **42**, 11 388 (1990).

¹⁵L. Nordheim, *Ann. Phys. (Leipzig)* **9**, 607 (1931).

¹⁶W. E. Spicer, J. A. Silberman, J. Morgen, I. Lindau, J. A. Wilson, A. B. Chen, and A. Sher, *Phys. Rev. Lett.* **49**, 948 (1982).

¹⁷P. Soven, *Phys. Rev.* **178**, 1136 (1969); B. Velický, S. Kirkpatrick, and H. Ehrenreich, *ibid.* **175**, 747 (1968).

¹⁸A.-B. Chen and A. Sher, *Phys. Rev. B* **17**, 4726 (1978); **23**, 5360 (1981); **19**, 3057 (1979); **23**, 5645 (1981).

¹⁹K. C. Hass, R. Lempert, and H. Ehrenreich, *Phys. Rev. Lett.* **52**, 77 (1984); R. Lempert, K. C. Hass, and H. Ehrenreich, *Phys. Rev. B* **36**, 1111 (1987).

²⁰S. Sakai and T. Sugano, *J. Appl. Phys.* **50**, 4143 (1979).

²¹(a) A. Kobayashi and A. Roy, *Phys. Rev. B* **35**, 5611 (1987); (b) A. Gonis, W. H. Butler, and G. M. Stocks, *Phys. Rev. Lett.* **50**, 1482 (1983).

²²F. Ducastelle, *J. Phys. C* **7**, 1795 (1974).

²³R. Alben, M. Blume, H. Krakauer, and L. Schwartz, *Phys. Rev. B* **12**, 4090 (1975); R. Alben, M. Blume, and M. Mckewon, *ibid.* **16**, 3829 (1977).

²⁴L. C. Davis, *Phys. Rev. B* **28**, 6961 (1983); L. C. Davis and H.

- Holloway, *Solid State Commun.* **64**, 121 (1987).
- ²⁵K. C. Hass, L. C. Davis, and A. Zunger, *Phys. Rev. B* **42**, 3757 (1990).
- ²⁶S. Lee, D. M. Bylander, and L. Kleinman, *Phys. Rev. B* **40**, 8399 (1989).
- ²⁷A. Zunger and J. E. Jaffe, *Phys. Rev. Lett.* **51**, 5662 (1983).
- ²⁸(a) D. J. Chadi, *Phys. Rev. B* **16**, 790 (1977); (b) S.-H. Wei and A. Zunger, *ibid.* **39**, 6279 (1988); **39**, 3279 (1989).
- ²⁹(a) M. F. Ling and D. J. Miller, *Phys. Rev. B* **34**, 7388 (1986); (b) S.-H. Wei and A. Zunger, *Appl. Phys. Lett.* **56**, 662 (1990); (c) J. E. Bernard and A. Zunger, *Phys. Rev. B* **36**, 3199 (1987).
- ³⁰A. Zunger, S.-H. Wei, L. G. Ferreira, and J. E. Bernard, *Phys. Rev. Lett.* **65**, 353 (1990).
- ³¹S.-H. Wei, L. G. Ferreira, J. E. Bernard, and A. Zunger, *Phys. Rev. B* **42**, 9622 (1990).
- ³²S.-H. Wei and A. Zunger, *Phys. Rev. B* **43**, 1662 (1991).
- ³³Z. W. Lu, S.-H. Wei, and A. Zunger, *Phys. Rev. B* (to be published).
- ³⁴J. Ihm, A. Zunger, and M. L. Cohen, *J. Phys. C* **12**, 4409 (1979).
- ³⁵G. Kerker, *J. Phys. C* **13**, L189 (1980).
- ³⁶D. M. Ceperley and B. J. Alder, *Phys. Rev. Lett.* **45**, 566 (1980).
- ³⁷J. P. Perdew and A. Zunger, *Phys. Rev. B* **23**, 5048 (1981).
- ³⁸S. Froyen, *Phys. Rev. B* **39**, 3168 (1989).
- ³⁹G. Lehman and M. Taut, *Phys. Status Solidi* **54**, 469 (1971).
- ⁴⁰P. N. Keating, *Phys. Rev.* **145**, B637 (1966).
- ⁴¹A. Zunger, *Phys. Rev. Lett.* **50**, 1215 (1983).
- ⁴²W. A. Harrison, *Electronic Structure and the Properties of Solids* (Dover, New York, 1989).
- ⁴³The LDA-calculated semirelativistic *s* orbital energies of Al, Ga, In, P, and As are -7.91 , -9.25 , -8.56 , -14.09 , and -14.77 eV, respectively. The *p* orbital energies are -2.86 , -2.82 , -2.78 , -5.68 , and -5.42 , respectively.
- ⁴⁴See S.-H. Wei and A. Zunger, *Phys. Rev. Lett.* **59**, 144 (1987), and references therein.
- ⁴⁵R. G. Dandrea and A. Zunger, *Appl. Phys. Lett.* **57**, 1031 (1990). Neglecting spin-orbit effects, the Γ_{5v} offset in the GaAs-GaP system is 0.52 eV and the Γ_{3v} offset is 0.12 eV, so their 2:1 average used here is 0.39 eV.
- ⁴⁶G. Martinez, in *Handbook on Semiconductors*, edited by M. Balkanski (North-Holland Amsterdam, 1980), Vol. 2, p. 181; A. Blacha, H. Presting, and M. Cardona, *Phys. Status Solidi B* **126**, 11 (1984).
- ⁴⁷(a) K. L. Tsang, J. E. Rowe, T. A. Callcott, and R. A. Logan, *Phys. Rev. B* **38**, 13 277 (1988); (b) K. C. Hass, *ibid.* **40**, 5780 (1989).
- ⁴⁸P. Boguslawski and A. Baldereschi, *Solid State Commun.* **70**, 1085 (1989).
- ⁴⁹A. A. Mbaye, *Solid State Commun.* **55**, 183 (1985).
- ⁵⁰K. R. Schulze, H. Neumann, and K. Unger: *Phys. Status Solidi* (b) **75**, 493 (1976); S. S. Vishnubhatla, B. Eyglunent, and J. C. Woolley, *Can. J. Phys.* **47**, 1661 (1969).
- ⁵¹O. Berolo and J. C. Woolley, *Can. J. Phys.* **49**, 1335 (1971); H. J. Lee, L. Y. Juravel, and J. C. Woolley, *Phys. Rev. B* **21**, 659 (1980); G. Oelgart, R. Schwabe, M. Heider, and B. Jacobs, *Semicond. Sci. Technol.* **2**, 468 (1987); T. F. Kuech, D. J. Wolford, R. Potemski, J. A. Bradley, K. H. Kelleher, D. Yan, J. P. Farrell, P. M. S. Lesser, and F. H. Pollak, *Appl. Phys. Lett.* **51**, 505 (1987).
- ⁵²C. Bosio, J. L. Staehli, M. Guzzi, G. Burri, and R. A. Logan, *Phys. Rev. B* **38**, 3263 (1988).
- ⁵³K. H. Goetz *et al.*, *J. Appl. Phys.* **54**, 4543 (1983).
- ⁵⁴See, for example, Table III in M. Bugajski, A. M. Kontkiewicz, and H. Mariette, *Phys. Rev. B* **28**, 7105 (1983).
- ⁵⁵A. Baldereschi and K. Maschke, *Solid State Commun.* **16**, 99 (1975).
- ⁵⁶S. J. Lee, H. S. Chung, K. Nahm, and C. K. Kim, *Phys. Rev. B* **42**, 1452 (1990).
- ⁵⁷D. Z.-Y. Ting and Y.-C. Chang, *Phys. Rev. B* **30**, 3309 (1984).
- ⁵⁸A.-B. Chen and A. Sher, *Phys. Rev. B* **22**, 3886 (1980).